Parkin interacting substrate zinc finger protein 746 is a pathological mediator in Parkinson's disease

Saurav Brahmachari,[1,2,3,*] Saebom Lee,[1,2,*] Sangjune Kim,[1,2,*] Changqing Yuan,[1,2,3] Senthilkumar S. Karuppagounder,[1,2,3] Preston Ge,[1,2,3] Rosa Shi,[1,2,3] Esther J. Kim,[1,2,3] Alex Liu,[1,2,3] Donghoon Kim,[1,2,5] Stephan Quintin,[1,2] Haisong Jiang,[1,2,3] Manoj Kumar,[1,2,3] Seung Pil Yun,[1,2,3] Tae-In Kam,[1,2,3] Xiaobo Mao,[1,2,3] Yunjong Lee,[1,2,3] Deborah A. Swing,[6] Lino Tessarollo,[6] Han Seok Ko,[1,2,5,‡] Valina L. Dawson[1,2,3,4,7,‡] and Ted M. Dawson[1,2,3,7,8,‡]

*,‡These authors contributed equally to this work.

α-Synuclein misfolding and aggregation plays a major role in the pathogenesis of Parkinson's disease. Although loss of function mutations in the ubiquitin ligase, parkin, cause autosomal recessive Parkinson's disease, there is evidence that parkin is inactivated in sporadic Parkinson's disease. Whether parkin inactivation is a driver of neurodegeneration in sporadic Parkinson's disease or a mere spectator is unknown. Here we show that parkin in inactivated through c-Abelson kinase phosphorylation of parkin in three α-synuclein-induced models of neurodegeneration. This results in the accumulation of parkin interacting substrate protein (zinc finger protein 746) and aminoacyl tRNA synthetase complex interacting multifunctional protein 2 with increased parkin interacting substrate protein levels playing a critical role in α-synuclein-induced neurodegeneration, since knockout of parkin interacting substrate protein attenuates the degenerative process. Thus, accumulation of parkin interacting substrate protein links parkin inactivation and α-synuclein in a common pathogenic neurodegenerative pathway relevant to both sporadic and familial forms Parkinson's disease. Thus, suppression of parkin interacting substrate protein could be a potential therapeutic strategy to halt the progression of Parkinson's disease and related α-synucleinopathies.

1 Neuroregeneration and Stem Cell Programs, Institute for Cell Engineering, Johns Hopkins University School of Medicine, Baltimore, MD 21205, USA
2 Department of Neurology, Johns Hopkins University School of Medicine, Baltimore, MD 21205, USA
3 Adrienne Helis Malvin Medical Research Foundation, New Orleans, LA 70130–2685, USA
4 Department of Physiology, Johns Hopkins University School of Medicine, Baltimore, MD 21205, USA
5 Diana Helis Henry Medical Research Foundation, New Orleans, LA 70130–2685, USA
6 Neural Development Section, Mouse Cancer Genetics Program, Center for Cancer Research, National Cancer Institute, Frederick, Maryland, USA
7 Solomon H. Snyder Department of Neuroscience, Johns Hopkins University School of Medicine, Baltimore, MD 21205, USA
8 Department of Pharmacology and Molecular Sciences, Johns Hopkins University School of Medicine, Baltimore, MD 21205, USA

Correspondence to: Ted M. Dawson
Neuroregeneration and Stem Cell Programs
Institute for Cell Engineering
Johns Hopkins University School of Medicine
733 North Broadway, Suite 731

Baltimore, MD 21205, USA
E-mail: tdawson@jhmi.edu

Correspondence may also be addressed to:
Han Seok Ko
E-mail: hko3@jhmi.edu

Valina L. Dawson
E-mail: vdawson@jhmi.edu

Introduction

Parkinson's disease is the second most common neurodegenerative disorder, that leads to a progressive loss of dopamine neurons in the substantia pars compacta (Dauer and Przedborski, 2003; Savitt et al., 2006). Accompanying the loss of dopamine neurons are motor symptoms that include a rest tremor, bradykinesias, and rigidity. Moreover, patients with Parkinson's disease have non-motor symptoms that include sleep disturbance, anxiety and depression and autonomic dysfunction among others (Bonnet et al., 2012). Late in the course of the disease, patients also develop cognitive symptoms that progress to dementia. Pathologically, most forms of Parkinson's disease have accumulation of α-synuclein (α-syn, encoded by *SNCA*) in structures designated as Lewy bodies and Lewy neurites throughout the nervous system (Goedert, 2001; Lee and Trojanowski, 2006; Goedert et al., 2013).

There are a number of genetic causes of Parkinson's disease including mutations in α-syn (Polymeropoulos et al., 1997; Kruger et al., 1998; Singleton et al., 2003; Chartier-Harlin et al., 2004; Zarranz et al., 2004) and LRRK2 (Zimprich et al., 2004; Di Fonzo et al., 2005, 2006; Ross et al., 2008), which cause autosomal dominant Parkinson's disease. In sporadic Parkinson's disease, α-syn misfolding and aggregation is thought to play a major role in the pathogenesis of the disease (Goedert, 2001; Maries et al., 2003; Lee and Trojanowski, 2006; Auluck et al., 2010; Goedert et al., 2013; Lashuel et al., 2013). Several α-syn transgenic mouse models of familial Parkinson's disease have been created and recapitulate most, if not all, the cardinal features of α-syn-induced neurodegeneration (Maries et al., 2003; Fernagut and Chesselet, 2004; Dawson et al., 2010; Chesselet and Richter, 2011; Lee et al., 2012; Bezard et al., 2013; Deng and Yuan, 2014). In addition, transgenic mouse models overexpressing familial Parkinson's disease-related mutated α-syn (A53T or A30P) have been established that show robust gastrointestinal dysfunction, a feature that precedes neurodegeneration in Parkinson's disease (Kuo et al., 2010). There are also mutations in E3 ubiquitin ligase parkin (encoded by *PRKN*) (Kitada et al., 1998), the kinase PINK1 (Valente et al., 2004) and the redox sensitive protein DJ1 (encoded by *PARK7*) (Bonifati et al., 2003). In addition there are a number of mutations or polymorphisms in other genes that are either causal or increase the risk of developing Parkinson's disease (Ramirez et al., 2006; Satake et al., 2009; Sidransky et al., 2009; Simon-Sanchez et al., 2009; Shulman et al., 2011; Vilarino-Guell et al., 2011; Zimprich et al., 2011; Hernandez et al., 2016). Parkin and PINK1 are linked in a common genetic pathway to regulate mitochondrial quality control (Fedorowicz et al., 2014; Eiyama and Okamoto, 2015; Fiesel et al., 2015). Although loss-of-function mutations in the E3 ubiquitin ligase parkin are a rare cause of autosomal recessive Parkinson disease (Kitada et al., 2007; Corti et al., 2011; Martin et al., 2011), there is evidence that parkin is also inactivated in the more common sporadic form of Parkinson's disease (Chung et al., 2004; Yao et al., 2004; Ko et al., 2005, 2010; LaVoie et al., 2005; Imam et al., 2011; Shin et al., 2011; Dawson and Dawson, 2014; Karuppagounder et al., 2014; Kurup et al., 2015; for a review see Panicker et al., 2017). However, whether parkin inactivation is a driver of the degenerative process of sporadic Parkinson's disease or a mere spectator is unknown. Here we evaluate the role of parkin inactivation and accumulation of parkin substrates in the pathogenesis of Parkinson's disease due to pathologic α-syn. We show that parkin is inactivated leading to the accumulation of parkin interacting substrate protein (PARIS) (zinc finger protein 746) (ZNF746) in two A53T α-syn transgenic models of familial Parkinson's disease and in the α-syn preformed fibril (PFF) model of sporadic Parkinson's disease. Moreover, knockout of PARIS prevents the neurodegeneration in these models providing evidence that parkin inactivation and accumulation of PARIS contribute significantly to the degenerative process initiated by pathological α-syn.

Materials and methods

Animals

The generation of transgenic (Tg) mice that overexpress human A53T α-syn using the mouse *PrnP* (mPrP) has been

described previously and are designated hA53T α-syn.G2–3 Tg (Lee et al., 2002). These mice were obtained from Jackson Laboratories (C57BL/6; Prnp-SNCA*A53T). PARIS knockout (KO) and conditional TetP-hA53T α-syn transgenic mice were generated and characterized in our laboratory as described below. Randomized mixed gender cohorts were used for all animal experiments. All mice were acclimatized for 3 days in the procedure room before starting any experiments. We aimed throughout to reduce animal suffering due to pain and discomfort. All procedures involving animals were approved by and conformed to the guidelines of the Institutional Animal Care Committee of Johns Hopkins University.

Antibodies

Primary antibodies used include the following: mouse anti-α-synuclein (610787; BD Transduction laboratories), mouse anti-α-synuclein, LB509 (ab27766; Abcam), rabbit anti-α-synuclein (2642; Cell Signaling), rabbit anti-pY245 c-Abl (2861; Cell Signaling), mouse anti-c-Abl (554148; BD Transduction Laboratories), mouse anti-pS129 α-synuclein (pSyn#64) (015–25191; Wako), rabbit anti-pY39 α-synuclein (Brahmachari et al., 2016), mouse anti-ubiquitin (MAB1510; Millipore), rabbit anti-GFAP (Z0334; Dako), rabbit anti-phosphotyrosine (610009; BD Transduction Laboratories), mouse anti-PARIS/ZNF746, Clone N196/16 (75–195; Antibodies Inc), mouse anti-PGC-1α (ST1202; Calbiochem), mouse anti-parkin (4211; Cell Signaling), rabbit anti-parkin (2132; Cell Signaling), rabbit anti-MFN1 (13798–1-AP; Proteintech), rabbit anti-ZNF746 (24543–1-AP; Proteintech), rabbit anti-PGC-1α (NBP1–04676; Novus), rabbit anti-phosphotyrosine (61–5800; ThermoFisher), rabbit anti-Bax (2772; Cell signaling), rabbit anti-RHOT1 (Miro1) (PA5–42646; ThermoFisher Scientific), rabbit anti-STEP61 (9069; Cell signaling), rabbit anti-NeuN (ab177487, Abcam), and rabbit anti-pS65 Ubiquitin (Fiesel et al., 2015) antibodies. Secondary antibodies used include the following: actin-peroxidase (Sigma), anti-rabbit and anti-mouse IgG (Santa Cruz), anti-phosphotyrosine, 4G10 platinum-peroxidase (Millipore) and peroxidase-linked species-specific whole antibody (GE health care).

Immunohistochemistry for mouse brain

Immunohistochemistry was carried out as described previously (Lee et al., 2013; Karuppagounder et al., 2014; Brahmachari et al., 2016). Mice were put into deep anaesthesia by intraperitoneal injection of pentobarbital (Nembutal) sodium solution [50 µl of 2-fold dilution in phosphate-buffered saline (PBS) of pentobarbital sodium 50 mg/ml, Lundbeck] and intracardially perfused with ice-cold PBS followed by 4% paraformaldehyde/PBS (wt/vol, pH 7.4). Brains were removed and post-fixed for 16 h in the same fixative. After cryoprotection in 30% sucrose/PBS (wt/vol, pH 7.4), brains were frozen on dry ice, and serial coronal sections (40 µm sections of brainstem, cerebellum, striatum or 60 µm sections of midbrain) were cut with a cryotome. Free-floating sections were blocked with 5% goat serum (vol/vol, Sigma-Aldrich)/PBS plus 0.2% Triton™ X-100 (vol/vol) and incubated with indicated antibodies, followed by incubation with biotin-conjugated secondary antibodies to

rabbit or mouse, ABC reagents (Vector Laboratories) and Sigmafast™ 3,3′-diaminobenzidine (DAB) tablets (Sigma-Aldrich). Sections were counterstained with Nissl (0.09% thionin, wt/vol) after desired antigen staining as described previously (Shin et al., 2011), followed by mounting with DPX (Sigma-Aldrich) before imaging under a microscope (Axiophot photomicroscope, Carl Zeiss Vision).

Quantitative analysis of immunohistochemistry

Every fourth serial section (60 µM for the substantia nigra region) was stained for tyrosine hydroxylase (TH) and counter stained with Nissl. TH-positive and Nissl-positive neurons from the substantia nigra pars compacta (SNpc) were counted through optical fractionators, an unbiased method for cell counting (West, 1993). This method was carried out using a computer-assisted image analysis system consisting of an Axiophot photomicroscope (Carl Zeiss Vision) equipped with a computer controlled motorized stage (Ludl Electronics), a HitachiHVC20 camera, and Stereo Investigator software (MicroBright-Field). The total number of TH-stained neurons and/or Nissl counts was calculated under $100\times$ (numerical aperture 1.4, coefficient of error 0.17) magnification (Shin et al., 2011; Lee et al., 2013). Serial striatal sections were processed for TH staining following the same procedure as above. Fibre density in the striatum was quantified by optical density (OD). ImageJ software (NIH) was used to analyse the OD as described previously (Lee et al., 2013).

Tissue lysate preparation

Tissue lysates were prepared as described previously (Lee et al., 2002; Brahmachari et al., 2016) with some modifications. Non-ionic detergent-soluble and insoluble fractions were made by homogenization of tissue in brain lysis buffer [10 mM Tris-HCl, pH 7.4, 150 mM NaCl, 5 mM EDTA, 0.5% Nonidet™ P-40, phosphatase inhibitor cocktail II and III (Sigma-Aldrich), and complete protease inhibitor mixture]. The homogenate was centrifuged (20 min at 4°C, 100 000g), and the resulting pellet (P1) and supernatant (S1, soluble) fractions were collected. The P1 was washed once in brain lysis buffer containing non-ionic detergent (0.5% Nonidet™ P-40) and the resulting pellet (P2, non-ionic detergent-insoluble) was homogenized in brain lysis buffer containing 1% SDS and 0.5% sodium deoxycholate. The homogenate was centrifuged and the resulting supernatant (non-ionic detergent-insoluble) was collected. Total lysates were prepared by homogenization of tissue in RIPA buffer [50 mM Tris, pH 8.0, 150 mM NaCl, 1% Nonidet™ P-40, 1% SDS, 0.5% sodium deoxycholate, phosphatase inhibitor cocktail II and III (Sigma-Aldrich), and complete protease inhibitor mixture]. The homogenate was centrifuged (20 min at 4°C, 100 000g), and the resulting supernatant was collected.

Immunoprecipitation and immunoblot analysis

For immunoprecipitation using mouse brains, tissues were homogenized and prepared in lysis buffer [10 mM Tris-HCl

(pH 7.4), 150 mM NaCl, 5 mM EDTA, 0.5% Nonidet™ P-40 (vol/vol), 1% Triton™ X-100, 0.5% sodium deoxycholic acid (wt/vol), Phosphatase inhibitor cocktail II and III (Sigma-Aldrich), and complete protease inhibitor mixture in PBS]. Protein levels in tissue lysates were quantified using a BCA protein assay kit (Pierce). The lysates were then rotated at 4°C for 1 h, followed by centrifugation at 18 000g for 20 min. The supernatants were then combined with 50 µl of Dynabeads™ Protein G (Life Technologies) preincubated with indicated antibodies, followed by rotating for 2 h or overnight at 4°C. Protein G was pelleted and washed four times using immunoprecipitation buffer or buffer with additional 500 mM NaCl, followed by three washes with PBS and samples were prepared by adding 2 × sample loading buffer (Bio-Rad). Immunoblot analysis or mouse brain samples using total, detergent-soluble or detergent-insoluble samples were performed as described previously (Lee *et al.*, 2002; Ko *et al.*, 2010; Brahmachari *et al.*, 2016). Brain tissue lysates or immunoprecipitated samples were electrophoresed on SDS-PAGE gels and transferred to nitrocellulose membranes. Membranes were blocked with 5% non-fat dry milk (wt/vol) in Tris-buffered saline with Tween-20 (TBS-T) and incubated with primary antibodies. After horseradish peroxidase-conjugated secondary antibody incubation, the immunoblot signal was detected using chemiluminescent substrates (Thermo Scientific).

Generation of PARIS knockout mice

To generate PARIS knockout (KO) mice, we used a targeting strategy to delete the zinc fingers by deleting the last three exons 5 to 7 and the 3′UTR, which were flanked by LoxP sites. The loss of 3′UTR destabilizes the *Znf746*/PARIS transcript (Supplementary Fig. 2A). The knockout of *Znf746*/PARIS was validated by PCR. The genotyping primers Y225 and Y226 were used for genotyping wild-type, and the size of the PCR product is 411 bp. For the knockout genotyping, the primers Y203 and Y203 were used and the PCR product size is 677 bp. The heterozygous mice show two bands (Supplementary Fig. 2B). The genomic deletion of PARIS was confirmed by Southern blot analysis (Supplementary Fig. 2C). Primers P204 and P205 were used to amplify the internal probe. Mouse genomic DNA was digested by SacI. Southern blot analysis confirmed the correct targeting with a 10 kb wild-type band and a 15 kb knockout band (Supplementary Fig. 2C, top). Primers P206 and P207 amplified the external 5′ probe. Mouse genomic DNA was digested by MfeI. Southern blot analysis confirmed the correct targeting with a 12.7 kb wild-type band and a 7.5 kb knockout band (Supplementary Fig. 2C, middle). Primers P208 and P209 amplified the external 3′ probe. Mouse genomic DNA was digested by HpaI. Southern blot analysis confirmed the correct targeting with an 8.4 kb wild-type band and a 5.7 kb knockout band (Supplementary Fig. 2C, bottom). Deletion of the *Znf746*/PARIS transcript was validated by RT-PCR (Supplementary Fig. 2D). The primer for reverse transcription was oligo dT. For PCR, primers Y233 and Y234 were used to amplify 164 bp band for wild-type and negative for knockout mice. RT-PCR was further confirmed by real-time PCR (Supplementary Fig. 2E). Finally, the deletion of the PARIS protein was confirmed by western blot analysis (Supplementary Fig. 2F).

Conditional TetP-hA53T α-syn transgenic mouse generation

To generate mPrP-TetP-human (h) A53T α-syn mice, the cDNA encoding human wild-type *SNCA* was subcloned into the unique XhoI site of the 9.0 kb mPrP-TetP vector (Supplementary Fig. 9A). Site-directed mutagenesis was conducted with the mPrP-TetP-hWT α-syn construct as a template to generate pPrP-TetP-hA53T α-syn construct (Supplementary Fig. 9A). The hA53T mutation was confirmed by DNA sequencing. The mPrP-TetP-hA53T α-syn construct was linearized by digestion with NoI1 and the purified linearized DNA fragment (7 kb) was used for pronuclear microinjection of single-cell embryos from B6C3F2 strain and the one or two cell embryos were transferred into B6D2F1 pseudo-pregnant female mice to produce founder mice. Microinjections were conducted by the National Cancer Institute Transgenic Core Facility. Founder animals were screened for transgene incorporation by PCR of tail genomic DNA using TetP-α-syn primers (Supplementary Fig. 9B and C) (Forward: 5′-CGGGTCGAGTAGGCGTGTAC-3′; Reverse: 5′-TCTAGATGATCCCCGGGTACCGAG-3′: PCR product: 173 bp). Positive founder mice with a high copy of number the transgene (hA53T-4360, hA53T-4299 and hA53T-4454) were crossed to hemizygous CamKIIα-tTA transgenic mice to drive hA53T α-syn protein expression *in vivo* (Supplementary Fig. 9D). Using this approach, we generated bigenic PrP-TetP-hA53T α-syn/CamKII α-tTA mice designated as CamK-hA53T (Supplementary Fig. 9D). We found that hA53T α-syn protein was overexpressed throughout the forebrain (hippocampus, cortex and striatum) and the ventral midbrain in the bigenic mice (Supplementary Fig. 9E and F). As the founder line hA53T-4360 expressed the highest level of α-syn (Supplementary Fig. 9E and F), it was selected for further characterization. The CamK-hA53T mice (line 4360) were used for AAV-tTA injections to drive hA53T α-syn protein expression in the ventral midbrain (Fig. 3, Supplementary Figs 9G and H, and 10–14).

Measurement of neurotransmitters in the striatum

Biogenic amine concentrations were measured by high performance liquid chromatography with electrochemical detection (HPLC-ECD). Briefly, mice were sacrificed by decapitation and the striatum was quickly removed. Striatal tissue was sonicated in 0.150 ml ice-cold 0.01 mM perchloric acid containing 0.01% EDTA and 60 ng 3,4-dihydroxybenzylamine (DHBA) as an internal standard. After centrifugation (15 000 g, 30 min, 4°C), the supernatant was passed through a 0.2 mm filter. Twenty microlitres of the supernatant were analysed in the HPLC column (4.6 mm 3 150 mm C-18 reverse phase column, Waters Atlantis T3) by a dual channel Coulochem III electrochemical detector (Model 5300, ESA, Inc). The protein concentrations of tissue homogenates were measured using the BCA protein assay kit (Pierce). Data were normalized to protein concentrations and expressed as nanograms or milligrams of protein (Karuppagounder *et al.*, 2014).

Stereotaxic intranigral virus injection

Stereotaxic injection was performed as described previously (Lee *et al.*, 2013). For stereotaxic injection of AAV1-IRES-zsGreen overexpressing tTA and zsGreen, 8-week-old mice of indicated genotypes were anaesthetized with pentobarbital (60 mg/kg). An injection cannula (26.5 gauge) was applied stereotaxically into the SNpc (anteroposterior, 3.2 mm from bregma; mediolateral, 1.3 mm; dorsoventral, 4.3 mm) unilaterally (applied into the right hemisphere). The infusion was performed at a rate of 0.2 μ/min, and 1 or 2 μl of a high-titre AAV1-tTA-IRES-zsGreen (3.5×10^{13} AAV vector genomes per ml in PBS) was injected into each mouse. After the final injection, the injection cannula was maintained in the substantia nigra for an additional 5 min for a complete absorption of the virus and then slowly removed from the mouse brain. The head skin was closed by suturing, and wound healing and recovery were monitored following surgery. For western blot analysis, brains were removed 1 month or 6 months after viral injection and lysates were prepared as described above. For stereological analysis, mice were perfused and fixed intracardially with ice-cold PBS followed by 4% paraformaldehyde (PFA) at 6 months after intranigral viral injection. The brain was processed for immunohistochemistry. Amphetamine-induced stereotypic rotation was performed at 6 months after the unilateral intranigral virus injection prior to sacrificing the mice.

Amphetamine-induced stereotypic rotation

Six months after mice received the AAV1-tTA intranigral injection into the right hemisphere, 5 mg/kg body weight amphetamine (Sigma-Aldrich) was administered intraperitonially. Mice were placed into a white paper cylinder of 20-cm diameter and monitored for 30 min. The behaviour of mice was recorded for at least 5 min between 20 and 30 min following amphetamine administration. Full body ipsilateral rotations (clockwise) were counted for each mouse from the video recordings. The animal genotypes were blinded and randomly used during the experiment and the blind was removed for final quantification and statistical assessment.

RT-PCR and real-time quantitative RT-PCR

Total RNA was extracted with TRIzol® reagent (Invitrogen), and cDNA was synthesized from total RNA (0.5 μg) using a First Strand cDNA synthesis kit (Invitrogen). Aliquots of cDNA were used as templates for RT-PCR and real-time qRT-PCR procedure. Relative quantities of mRNA expression were analysed using real-time PCR (Applied Biosystems ViiA™ 7 Real-Time PCR System). The SYBR® GreenER™ reagent (Invitrogen) was used according to the manufacturer's instruction. Primer sequences for RT-PCR are as follows: PARIS (*Znf746*), forward 5′-AGTTGGACTCTGGAGCAGGA-3′, reverse 5′- GCTGCTGTGTTGAGCTTCAG-3′; parkin (*Prkn*), forward 5′-TGGAAAGCTCCGAGTTCAGT-3′, reverse 5′-CCTTGTCTGAGGTTGGGTGT-3′; *Aimp2*, forward 5′-ACCAGGTAAAGCCCTATCATGG-3′, reverse 5′-GAGCCGGTACATGCAGGTT-3′; *Gapdh*, forward 5′- AGGTC

GGTGTGAACGGATTTG-3′, reverse 5′- TGTAGACCATGTAGTTGAGGTCA-3′. Primer sequences for RT-PCR and Southern blot analysis for characterization of PARIS knockout mice are as follows: Y233, 5′-GGGACACTGAAGCTCAACACAGCAG -3′; Y234, 5′- GGGAAGAATCTTGTGGCTTGGCCTG-3′; P204, 5′-GAAAAGCACAGGTGCTTCTC-3′; P205, 5′-GGGCATAAAATTGTGAAGCTTC-3′; P206, 5′-CTCTATCCCATCAACCCAGAAG-3′; P207, 5′-GTGTTAGCCATAAAACTACAGAGTG-3′; P208, 5′-GTGTTAGCCATAAAACTACAGAGTG-3′; P209, 5′-GAGTTCTTGGGTATTTAAGCATGC-3′.

Southern blot

Southern blot analysis was performed with DIG-High prime DNA labelling and Detection starter kit II (Roche #11585614910), as follows. The internal probe, external 5′ probe and external 3′ probe were amplified with primers P204/205, P206/207 and P208/209, respectively. All the probes were purified and labelled with digoxigenin-11-dUTP using DIG-High Prime. Mouse genomic DNA was isolated, purified and digested by SacI, MfeI and HpaI, respectively. Digested DNA was loaded to 1% agarose gel and run at 20 V overnight. DNA denaturation and gel neutralization were performed by standard protocols. DNA was transferred and fixed to positively-charged nylon membranes (Roche #11209299001). DNA hybridization and detection were performed as described in the kit instructions. A wild-type band of 10 kb, and a knockout band of 15 kb are expected with the internal probe and SacI digestion; a wild-type band of 12.7 kb and a knockout band of 7.5 kb are expected with the external 5′ probe and MfeI digestion; and a wild-type band of 8.4 kb knockout band of 5.7 kb are expected with the external 3′ probe and HpaI digestion. All the primer sequences are listed in the 'RT-PCR and real-time quantitative RT-PCR' section.

α-Syn preformed fibril preparation

Purification of recombinant of α-syn proteins and *in vitro* fibril generation was performed as published (Mao *et al.*, 2016). Assembly reactions of α-syn were performed by continuous agitation of α-syn for 7 days in an amber glass vial with a magnetic stirrer (10*g* at 37°C). α-Syn PFFs were harvested and evaluated for the quality of the fibrils. To avoid repeated freeze and thaw, the PFFs were aliquoted and stored at −80°C.

Stereotaxic procedure for α-syn preformed fibril injection

Stereotaxic procedure was performed as described previously (Mao *et al.*, 2016). On the day of intrastriatal injections, preparations were diluted in sterile PBS and briefly sonicated in a temperature controlled sonicator waterbath. Two-month-old mice were anaesthetized with pentobarbital and PBS, recombinant α-syn PFF (5 μg/2 ml) or recombinant α-syn monomer (5 μg/2 ml) was stereotactically delivered into one striatum. The following reference coordinates for the dorsal neostriatum were used: + 0.2 mm medial-lateral (ML); + 2.0 mm antero-posterior (AP) and + 2.8 mm dorso-ventral (DV) from bregma. Injections were performed using a 2 μl syringe (Hamilton) at a rate of 0.1 μl/min with the needle left in

place for $\geqslant 5$ min before slow withdrawal of the needle. After surgery, animals were monitored and post-surgical care was provided. Animal behaviour studies were performed at 180 days and mice were euthanized for biochemical, neurochemical and histological studies. For biochemical studies, tissues were immediately frozen after removal and stored at $-80°C$. For histological studies, mice were perfused transcardially with PBS and 4% PFA and brains were removed, followed by overnight fixation in 4% PFA and transfer to 30% sucrose for cryoprotection.

Behavioural tests

Open-field test

The Open-field test was performed by placing of animals into an infrared beam chamber. Activity was monitored using the Photobeam Activity System (San Diego Instruments), which provides a grid of infrared beams. The total number of beam breaks over a period of 30 min was recorded and analysed.

Pole test

The Pole test was performed as described previously (Mao *et al.*, 2016). A 9-mm diameter 2.5-foot metal rod wrapped with bandage gauze was used as the pole. Mice were placed on the top of the pole (3 inches from the top of the pole) facing head-up. The time taken to turn and total time taken to reach the base of the pole was recorded. Before the actual test the mice were trained for two consecutive days and each training session consisted of three test trials. The maximum cut-off time to stop the test was 120 s. Results were expressed in turn and total time (in seconds) (Mao *et al.*, 2016).

Grip strength test

The grip strength test was performed as described before (Mao *et al.*, 2016). Neuromuscular strength was measured by maximum holding force generated by the mice (Bioseb). Mice were allowed to grasp a metal grid with either their fore and/or hind limbs or both. The tail was gently pulled, and the maximum holding force recorded by the force transducer when the mice released their grasp on the grid. The peak holding strength was digitally recorded and displayed as force (in grams) (Mao *et al.*, 2016).

Rotarod test

The rotarod test was performed as described previously (Yun *et al.*, 2018). Briefly, the mice were trained on the rotarod apparatus three consecutive days before the test. Mice were placed on a rotating rod (4 rpm) and then tested for the accelerating trial of 5 min with the speed changing from 4 to 40 rpm. The latency to fall from the rod was recorded and data were presented as mean latency from three trials under blind condition to different groups.

Cylinder test

The cylinder test has been designed to measure spontaneous movement in rodents placed in a novel environment (Yun *et al.*, 2018). The mice were monitored for asymmetry in spontaneous forelimb use by being placed in a small transparent cylinder 14.5 cm in diameter and 20.5 cm in height. Independent use of the ipsilateral or contralateral forelimb for contacting the vertical surface of the cylinder was measured

in at least 20 exploratory movements over a 10-min recording. The number of ipsilateral forelimb contacts was expressed as a percentage of the total forelimb contracts.

Statistics

All data were analysed using GraphPad Prism 6 software. Data were presented as mean ± standard error of the mean (SEM) with at least three biologically independent experiments. Unpaired two-tailed Student's *t*-tests, one-way ANOVA, or two-way ANOVA followed by Sidak's or Tukey's multiple comparisons test were used to assess the statistical significance. Assessments with $P < 0.05$ were considered significant. Statistical analysis for the survival curves was performed by the Mann-Whitney-Wilcoxon test.

Data availability

Authors declare that data supporting the findings of this study are included in this manuscript and additional supporting data are available from the corresponding authors upon reasonable request.

Results

Human A53T α-synuclein overexpression triggers c-Abl activation and impairment of parkin activity

Parkin undergoes auto-ubiquitination, and this self-ubiquitination of parkin reflects its ubiquitination activity (Imai *et al.*, 2000; Zhang *et al.*, 2000; Ko *et al.*, 2010). To determine whether parkin activity is reduced in the setting of α-syn-induced neurodegeneration, we carried out a time-course study of the levels of auto-ubiquitinated parkin as a measure of the activation state of parkin in the G2–3 line of the mouse prion promoter human A53T (hA53T) α-syn transgenic mouse (hA53T α-syn.G2–3 Tg), which constitutively expresses hA53T α-syn (Lee *et al.*, 2002). The levels of ubiquitinated parkin decrease at 6 months and remain depressed for the remainder of the lifespan of the hA53T α-syn.G2–3 Tg mice, while the total parkin levels remain constant (Fig. 1A and B). Coincident with the reduced levels of auto-ubiquitinated parkin, is the activation of the stress-activated non-receptor tyrosine kinase, c-Abl as assessed by phosphorylation of c-Abl on Y245 (pY245 c-Abl) (Brasher and Van Etten, 2000), and tyrosine phosphorylation (pY143) of parkin (Fig. 1A and C), which is known to prevent parkin activation (Ko *et al.*, 2010; Imam *et al.*, 2011; Panicker *et al.*, 2017). At 6 months of age, pY143 parkin levels peak and begin to decrease in early symptomatic (7 to 8 months of age) hA53T α-syn.G2–3 Tg mice and the levels are reduced further in the late symptomatic stage (Fig. 1A and C). What accounts for this reduction in pY143 levels is not known. However, pY143 parkin levels at the late symptomatic stage hA53T α-syn.G2–3 Tg mice are still higher than the levels in age-matched non-
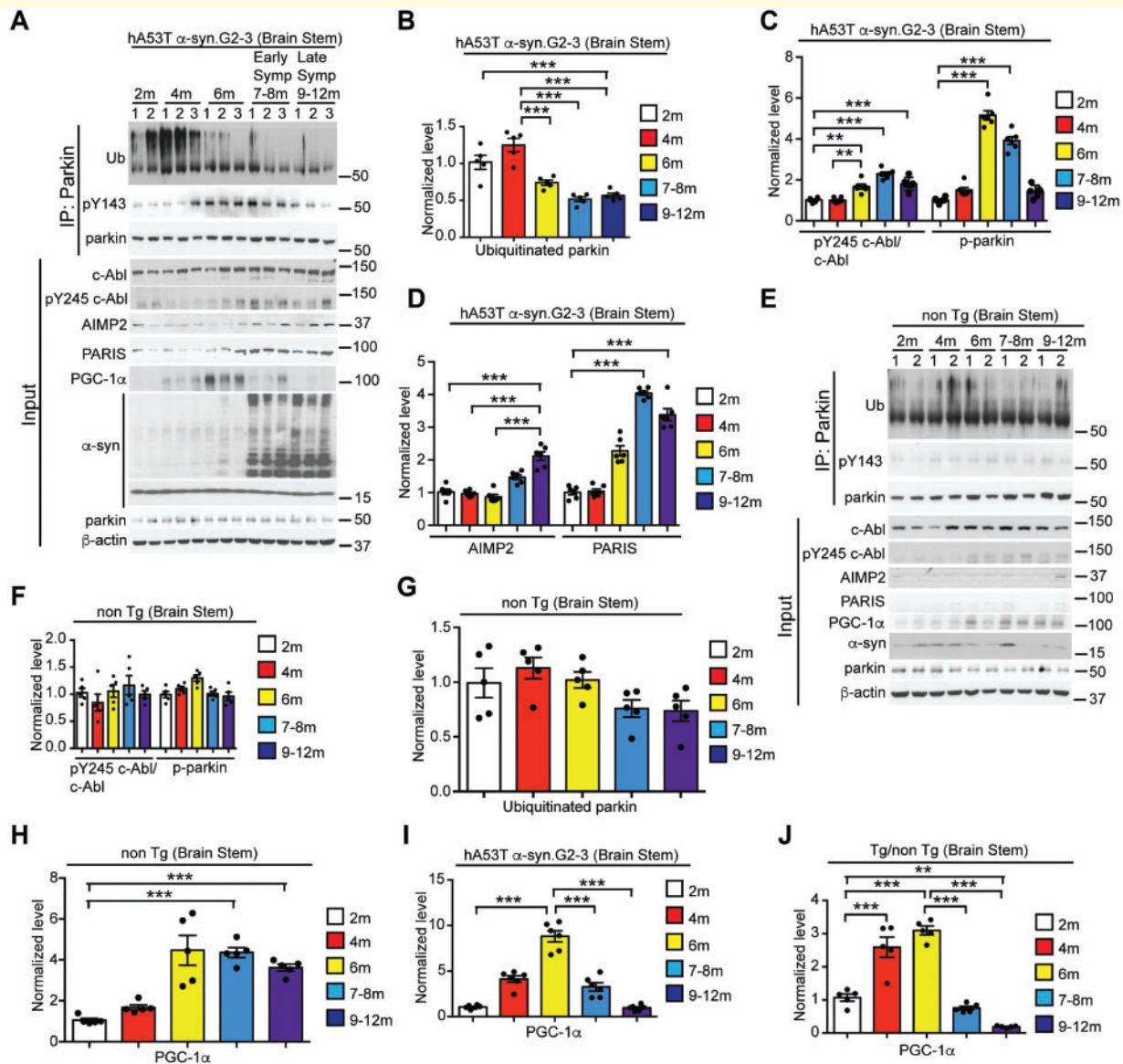
Figure 1 Ageing leads to c-Abl overactivation, parkin inactivation, and accumulation of parkin substrates in hA53T αsyn.G2–3 Tg mice. (A and E) Anti-parkin immunoprecipitation samples from the brainstem lysates of (A) hA53T α-syn.G2–3 mice and (E) non-transgenic (non-Tg) mice were immunoblotted with anti-ubiquitin to monitor ubiquitinated parkin, anti-phosphotyrosine to monitor tyrosine-phosphorylated (pY143) parkin, and anti-parkin antibodies to show immunoprecipitated parkin. The input samples from (A) hA53T α-syn.G2–3 transgenic and (E) non-transgenic mice immunoblotted with anti-c-Abl, anti-pY245 c-Abl, anti-AIMP2, anti-PARIS, anti-PGC-1α, and anti-α-syn antibodies to monitor their levels and anti-β-actin antibody was used as a loading control. The designated sample numbers in A and E indicate individual experimental animals. (B and G) Quantification of auto-ubiquitinated parkin normalized to immunoprecipitated parkin in A and E. (C and F) Quantifications of pY245 c-Abl protein levels normalized to c-Abl and tyrosine-phosphorylated (pY143) parkin normalized to immunoprecipitated parkin in A and F. (D) Quantifications of AIMP2 and PARIS protein levels normalized to β-actin in A and F. (H and I) Quantifications of PGC-1α protein levels normalized to β-actin in A and E. (J) Quantifications of PGC-1α protein levels in hA53T αsyn.G2–3 Tg in H normalized to PGC-1α protein levels in non-transgenic mice in I. Data are from three independent experiments. Statistical significance was determined by one-way ANOVA with Sidak's post-test of multiple comparisons. Quantified data are expressed as mean ± SEM *$P < 0.05$, **$P < 0.01$, ***$P < 0.001$.

transgenic mice (Figs 1A, E, 2 and 3), which is consistent with parkin inactivity in symptomatic hA53T α-syn.G2–3 Tg mice. Accompanying the inactivation of parkin is an elevation of the pathogenic parkin substrates, AIMP2 (aminoacyl tRNA synthetase complex interacting multifunctional protein 2) (Corti *et al.*, 2003; Ko *et al.*, 2010;

Imam *et al.*, 2011; Lee *et al.*, 2013) and the parkin interacting substrate (ZNF746/PARIS) (Shin *et al.*, 2011; Stevens *et al.*, 2015; Lee *et al.*, 2017) (Fig. 1A and D) similar to the elevation in the substantia nigra of sporadic Parkinson's disease (Ko *et al.*, 2010; Imam *et al.*, 2011; Shin *et al.*, 2011; Lee *et al.*, 2013). There is a significant
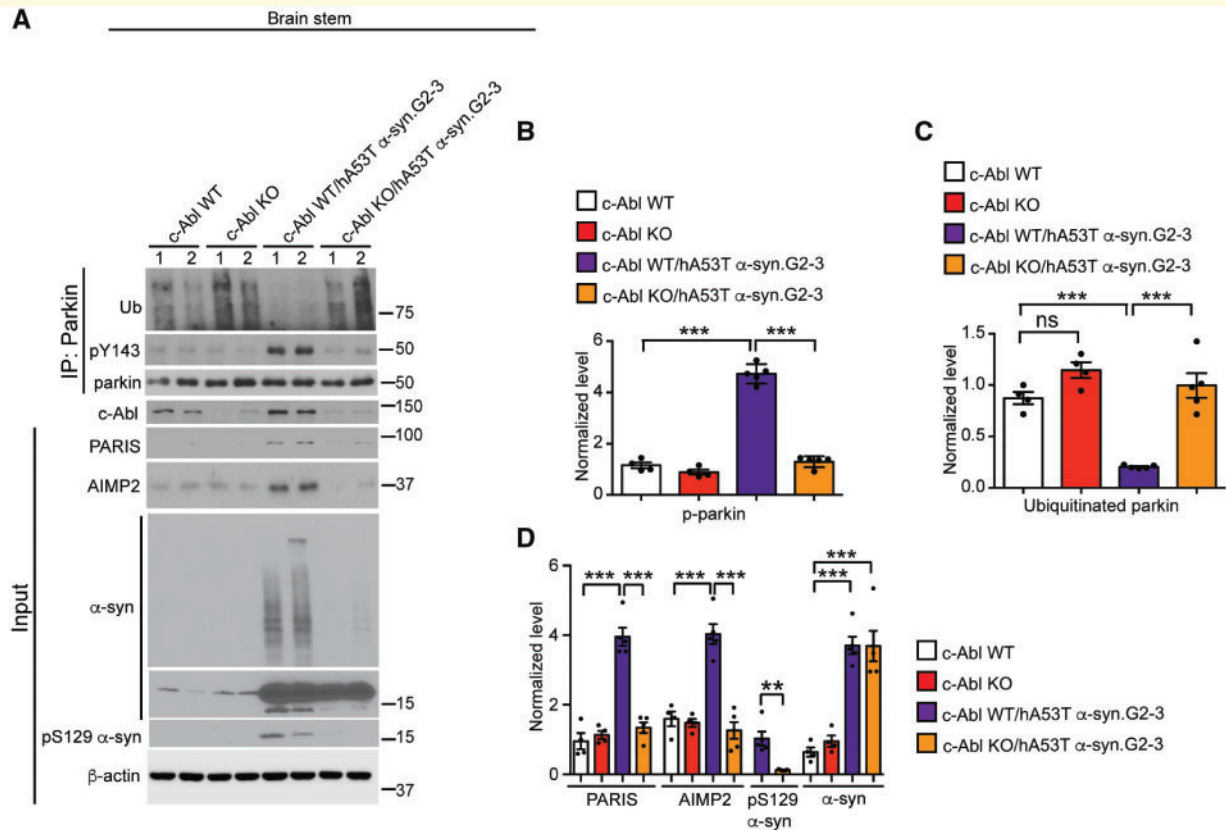
Figure 2 c-Abl knockout rescues parkin activity and reduces PARIS and AIMP2 levels in hA53T αsyn.G2–3 Tg mice.
(**A**) Representative immunoblots of ubiquitin, pY143 parkin, and parkin from anti-parkin immunoprecipitation samples of brainstem lysates and c-Abl, PARIS, AIMP2, α-syn, pS129 α-syn and β-actin in the brainstem lysates from age-matched c-Abl wild-type, C-Abl KO, symptomatic c-Abl wild-type/hA53T αsyn.G2–3 Tg mice and c-Abl KO/hA53T αsyn.G2–3 Tg mice littermates. The designated sample numbers indicate individual experimental animals. (**B–D**) Quantifications from **A** for (**B**) pY143 parkin and (**C**) ubiquitinated parkin levels normalized to immunoprecipitated parkin, and (**D**) PARIS, AIMP2 and α-syn protein levels normalized to β-actin, and pS129 α-syn protein level normalized to α-syn. Data are from three independent experiments. Statistical significance was determined by one-way ANOVA with Sidak's post-test of multiple comparisons. The data are presented as the mean ± SEM. $*P < 0.05$, $***P < 0.001$; ns = not significant; WT = wild-type.

2-fold upregulation of PARIS at 6 months, coincident with the tyrosine phosphorylation and inactivation of parkin (Fig. 1A and D). Two months later, during the early symptomatic stage of the hA53T α-syn.G2–3 Tg mice, AIMP2 is significantly upregulated 1.5-fold while PARIS is upregulated 4-fold (Fig. 1A and D). AIMP2 is further upregulated 2-fold at the late symptomatic stage (Fig. 1A and D). In non-transgenic mice, there is mild, but non-significant increase in the pY245 c-Abl level in older mice (Fig. 1E and F). Tyrosine phosphorylation of parkin is low and does not change with age (Fig. 1E and F). The auto-ubiquitination state of parkin (Fig. 1 E and G) remains relatively unchanged and the levels of the parkin substrates AIMP2 and PARIS are barely detectable in the non-transgenic mice age (Fig. 1E). As PARIS is a transcriptional repressor and one of its targets is peroxisome proliferator-activated receptor gamma coactivator 1 alpha (PGC-1α) (Shin et al., 2011; Scarffe et al., 2014; Siddiqui et al., 2015, 2016; Stevens et al., 2015; Lee et al., 2017), the levels of PGC-1α were assessed at 2, 4, 6, 7–8 and 9–12

months of age. Interestingly, the levels of PGC-1α increase with age in the non-transgenic and the hA53T α-syn.G2–3 Tg mice up to 6 months of age (Fig. 1A, E, H and I). In the non-transgenic mice, the levels PGC-1α remain elevated while the levels of PGC-1α are reduced in the early and late symptomatic hA53T α-syn.G2–3 Tg mice (Fig. 1A, E, H and I). The relative levels of PGC-1α in the hA53T α-syn.G2–3 Tg mice with respect to non-transgenic increase with age up to 6 months, then the levels reduce dramatically. At the late symptomatic stage, the levels of PGC-1α are significantly reduced compared to 2 months of age (Fig. 1J). At the late end stage of the hA53T α-syn.G2–3 Tg mice, c-Abl is activated, parkin is tyrosine phosphorylated and inactivated, AIMP2 and PARIS levels are increased, and PGC-1α levels are reduced in areas of pathology including the brainstem (Supplementary Fig. 1A–C) and spinal cord (Supplementary Fig. 1D–F) but not the cortex (Supplementary Fig. 1G–I) of the hA53T α-syn.G2–3 Tg mice compared to non-transgenic mice. The cortex is relatively spared from pathology in the hA53T α-syn.G2–3 Tg

mice (Lee et al., 2002; Brahmachari et al., 2016). To rule out the possibility that changes in mRNA levels of Znf746/PARIS and Aimp2 contribute to their increase in protein levels, we examined the mRNA expressions of Znf746/PARIS and Aimp2 by qPCR analysis (Supplementary Fig. 1J and K). No significant differences in mRNA levels of Znf746/PARIS (Supplementary Fig. 1J) and Aimp2 (Supplementary Fig. 1K) were observed among young (2 month) and symptomatic (10 month) hA53T α-syn.G2–3 Tg mice as well as age-matched non-transgenic controls. We also examined the mRNA level of Prkn/parkin and expectedly, there was no significant change in the level among the ages and genotypes as mentioned above (Supplementary Fig. 1L).

c-Abl mediates loss of parkin activity and accumulation of PARIS and AIMP2 in hA53T α-syn.G2–3 Tg mice

As c-Abl tyrosine phosphorylation and inactivation of parkin leads to an accumulation of parkin substrates (Ko et al., 2010; Imam et al., 2011), we assessed the activation state of parkin and the levels of AIMP2 and PARIS in 10–12-month-old hA53T α-syn.G2–3 Tg mice on a c-Abl knockout (c-Abl-KO) background (Brahmachari et al., 2016). Knockout of c-Abl in the hA53T α-syn.G2–3 Tg mice (c-Abl-KO/hA53 α-syn.G2–3 Tg mice) restores parkin activity as measured by the reduction of pY143 parkin and an increase in auto-ubiquitinated parkin levels (Fig. 1A–C), as well as restoration of the levels of PARIS and AIMP2 equivalent to those in non-transgenic mice (Fig. 2A and D). Accompanying these changes in the c-Abl-KO/hA53T α-syn.G2–3 Tg mice is a reduction in pathological α-syn as observed by abrogation of high molecular weight species of α-syn and pS129 α-syn (Fig. 2A and D) (Brahmachari et al., 2016). These results, taken together, indicate that parkin is maintained in an inactivated state via tyrosine phosphorylation by c-Abl in the hA53T α-syn.G2–3 Tg mice, which leads to the accumulation of the parkin pathogenic substrates, PARIS and AIMP2.

Generation and characterization of PARIS knockout mice

The embryonic lethality of the AIMP2 knockout mice (Kim et al., 2003) prevents a determination of whether AIMP2 plays a role in α-syn-induced neurodegeneration. To determine whether PARIS plays a role, PARIS knockout (PARIS KO) mice were generated (Supplementary Fig. 2). A targeting strategy deleting the zinc fingers was used in which the last three exons of PARIS were flanked with loxP sites (Supplementary Fig. 2A). Genomic deletion of Znf746/PARIS was achieved by breeding PARIS-targeted mice to male germ-line protamine-Cre mice (O'Gorman et al., 1997). PCR confirms the knockout of PARIS

(Supplementary Fig. 2B). Southern blot analysis confirms the successful targeting with wild-type bands and targeted bands as indicated (Supplementary Fig. 2C). RT-PCR confirms the absence of the targeted RNA (Supplementary Fig. 2D). Real-time Q-PCR analysis shows that Znf746/PARIS mRNA is absent in PARIS KO mice (Supplementary Fig. 2E). Immunoblot analysis reveals the loss of protein expression in the PARIS KO animal (Supplementary Fig. 2F). The knockout mice were backcrossed for more than 10 generations. Homozygous PARIS KO mice are viable and live a normal life-span compared to wild-type littermates (Supplementary Fig. 3A). No significant difference in body weight was observed among PARIS KO and wild-type littermates (Supplementary Fig. 3B). No gross developmental or behavioural defects were observed between PARIS KO and wild-type littermates (data not shown). There were also no obvious abnormalities in other tissues as accessed by pathological necropsy of heart, lung, spleen, kidney, thymus, liver, intestine, gonad, eyes and cerebrum (data not shown). No discernible difference was observed in the hippocampal neurons between wild-type and PARIS KO mice as assessed by NeuN staining (Fig. 3C). Stereological assessment of TH and Nissl-stained dopamine neurons in the SNpc did not reveal any difference between PARIS KO and wild-type littermate mice (Supplementary Fig. 3D and E). There was also no difference in dopamine or its metabolites as assessed by high performance liquid chromatography (HPLC) (Supplementary Fig. 3F and G).

PARIS plays a key role in α-syn-induced neurodegeneration in hA53T α-syn.G2–3 Tg mice

The PARIS KO mice were cross-bred to the hA53T α-syn.G2–3 Tg mice to create Znf746/PARIS$^{+/-}$ and Znf746/PARIS$^{+/-}$/hA53T α-syn.G2–3 Tg mice, which were then cross-bred to each other. From this cross breeding, littermates with the following genotypes: PARIS wild-type, PARIS KO, hA53T α-syn.G2–3, and PARIS KO/hA53T α-syn.G2–3 were separated and aged (Fig. 3A); and survival was monitored. The hA53T α-syn.G2–3 Tg mice live an average of 10 months (Lee et al., 2002; Brahmachari et al., 2016) with survival prolonged by 5 months in a PARIS KO background (Fig. 3B). Open field monitoring at 6 months of age revealed a significant increase in horizontal and vertical activity in hA53T α-syn.G2–3 Tg mice (Unger et al., 2006; Brahmachari et al., 2016), which was significantly reduced in the PARIS KO/hA53T α-syn.G2–3 Tg mice (Fig. 3C). The different cohorts of mice were assessed for expression levels of PARIS, PGC-1α, c-Abl, pY245 c-Abl, parkin, AIMP2, α-syn, and pS129α-syn in the brainstem (Fig. 3D, E and G–J), spinal cord (Supplementary Fig. 4A and B) and cortex (Supplementary Fig. 4C and D) at end stage (9–12 months). In addition, parkin and pY143 parkin levels were examined via immunoprecipitation followed by immunoblot analysis
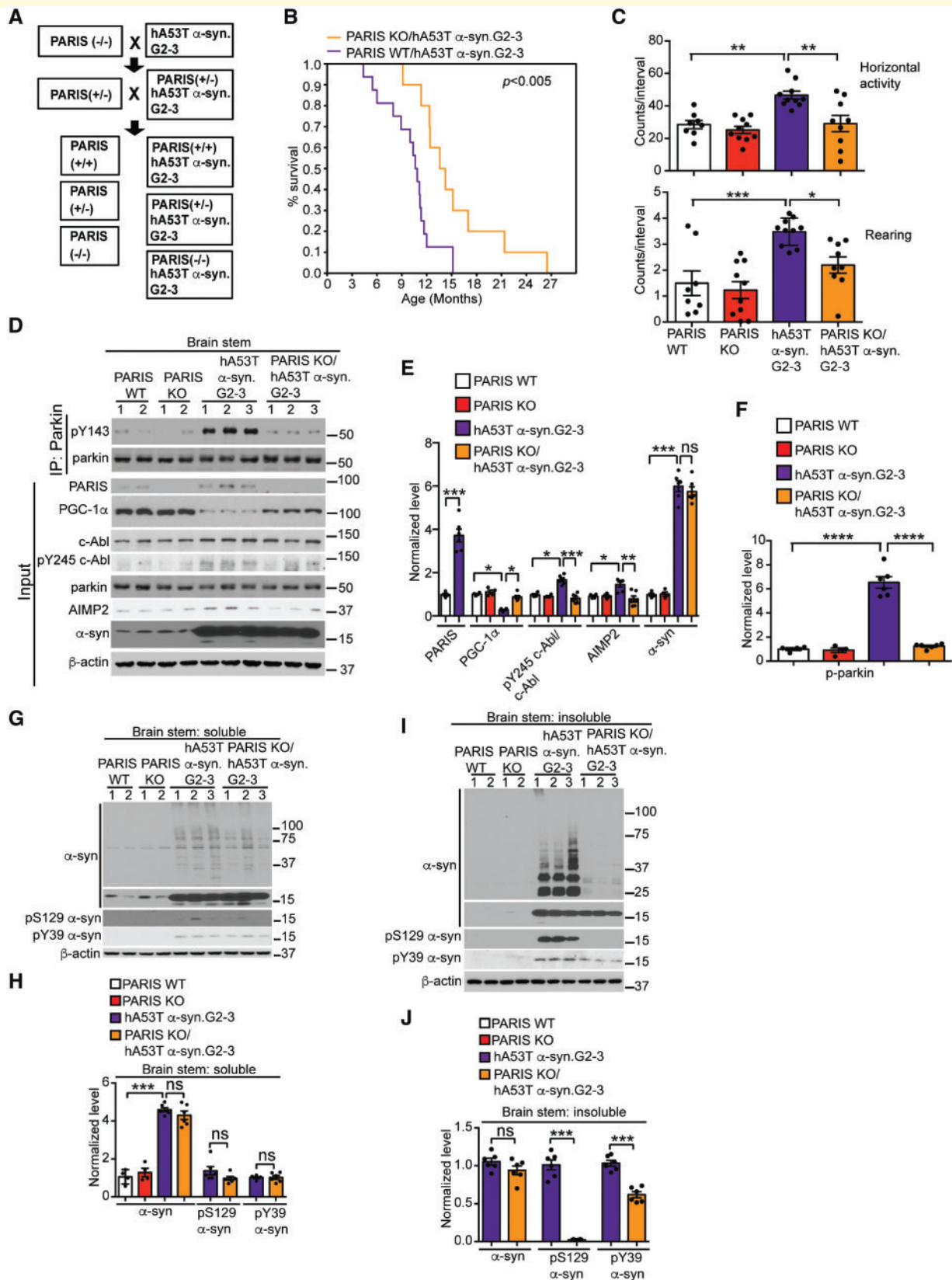
Figure 3 PARIS deletion extends survival and reduces behavioural deficits, alters c-Abl and parkin activity and AIMP2 and PGC-1α levels, and reduces α-syn neurodegeneration in hA53T αsyn.G2–3 Tg mice. (**A**) Breeding strategy to generate PARIS KO/ hA53T αsyn.G2–3 Tg mice. (**B**) Kaplan-Meier survival curve analysis for PARIS wild-type/hA53T αsyn.G2–3 Tg and PARIS KO/ hA53T αsyn.G2–3 Tg mice (n = 20–30 mice per group) statistical analysis was performed by Mann-Whitney-Wilcoxon test. $P < 0.01$. (**C**) Open field novelty-induced horizontal (*top*) and vertical (*bottom*) activities in cohorts of 8–10 mice per group at 6 months of age for PARIS wild-type, PARIS KO, hA53T

in the brainstem (Fig. 3D and F). Equivalent levels of α-syn were expressed among hA53T α-syn.G2–3 Tg mice and PARIS KO/hA53T α-syn.G2–3 Tg mice. PARIS was barely detectable in wild-type mice and was elevated over 3-fold in hA53T α-syn.G2–3 Tg brainstem (Fig. 3D and E), and over 7-fold in the spinal cord (Supplementary Fig. 4A and B). PARIS was absent in the PARIS KO and the PARIS KO/hA53T α-syn.G2–3 Tg mice (Fig. 3D and Supplementary Fig. 4A and C). pY245 c-Abl, AIMP2 and PARIS were elevated in the brainstem (Fig. 3D and E) and spinal cord (Supplementary Fig. 4A and B), but not in the cortex (Supplementary Fig. 4C and D) of hA53T α-syn.G2–3 Tg mice, and knockout of PARIS markedly reduces pY245 c-Abl and AIMP2 in hA53T α-syn.G2–3 Tg mice (Fig. 3D, E and Supplementary Fig. 4A and B). PGC-1α levels were reduced in the hA53T α-syn.G2–3 Tg mice in the brainstem and spinal cord (Fig. 3D, E and Supplementary Fig. 4A and B), but not in the cortex (Supplementary Fig. 4C and D) and the levels were restored in the PARIS KO/hA53T α-syn.G2–3 Tg mice (Fig. 3D, E and Supplementary Fig. 4A and B). pY143 parkin was markedly elevated in the brainstem of hA53T α-syn.G2–3 Tg mice, and PARIS deletion restores its level (Fig. 3D and F). There was no change in parkin levels in the brainstem among the different genotypes (Fig. 3D). The brainstem of the different genotypes was fractionated into detergent-soluble (Fig. 3G and H) and insoluble fractions (Fig. 3I and J). Immunoblot of these fractions demonstrates that in the hA53T α-syn.G2–3 Tg mice there is accumulation of insoluble pS129 α-syn, pY39 α-syn and high molecular weight species of α-syn. No abnormalities were observed in the other genotypes (Fig. 3I and J). Mild accumulation of soluble pS129 α-syn, pY39 α-syn and high molecular weight species of α-syn, as well as proteolytic fragments of α-syn, were detected in hA53T α-syn Tg and PARIS KO/hA53T α-syn.G2–3 Tg mice, but no significant difference in their levels was observed among them (Fig. 3G and H). PARIS KO significantly reduces the levels of insoluble pS129 α-syn, pY39 α-syn and high molecular weight species of α-syn (Fig. 3I and J).

In symptomatic hA53T α-syn.G2–3 Tg mice there was substantial neuronal accumulation of human pS129 α-syn

in a number of brain regions, including the brainstem and cerebellum (Supplementary Fig. 4E). There was a prominent accumulation of ubiquitin in neurites and cell bodies in all affected regions (Supplementary Fig. 4F) and substantial GFAP immunoreactivity in the symptomatic hA53T α-syn.G2–3 Tg mice (Supplementary Fig. 4G). There was no significant accumulation of pS129 α-syn, ubiquitin or GFAP in any of the other age-matched mouse genotypes (Supplementary Fig. 4E–G). PARIS KO substantially reduces the accumulation of human pS129 α-syn, ubiquitin and GFAP immunoreactivity (Supplementary Fig. 4E–G). Taken together, our results indicate that PARIS is a critical mediator of familial Parkinson's disease-relevant A53T α-syn-induced neurodegeneration.

Generation of tetracycline inducible mouse model of human A53T α-syn (TetP-hA53T α-syn)

Although the hA53T α-syn.G2–3 Tg mice exhibit most, if not all the features of α-synuncleinopathy degeneration, they do not exhibit loss of dopamine neurons (Lee *et al.*, 2002). To determine whether c-Abl regulates parkin activity and subsequent accumulation of PARIS and AIMP2, and, if PARIS plays a role in the loss of dopamine neurons due to overexpression of hA53T α-syn, we generated a tetracycline inducible mouse model of human A53T α-syn (TetP-hA53T α-syn) (Supplementary Fig. 5A). The relative copy number of the TetP-hA53T α-syn transgenic was assessed via PCR (Supplementary Fig. 5B and C). From 34 founders, the three TetP-hA53T α-syn lines with the highest copy number were selected for further characterization by breeding to CamKIIα-tTA transgenic mice to identify animals that expressed high levels of hA53T α-syn protein expression *in vivo* (Supplementary Fig. 5D). We found that hA53T α-syn protein was overexpressed throughout the forebrain (hippocampus, cortex and striatum) and the ventral midbrain of the bigenic TetP-hA53T α-syn/CamKII α-tTA (CamK-hA53T α-syn) mice (Supplementary Fig. 5E and F). The CamK-hA53T mouse line 4360 (CamK-4360) expressed the highest level of hA53T α-syn (Supplementary Fig. 5E and F) and was

---

Figure 3 Continued

α-syn.G2–3 Tg and PARIS KO/ hA53T α-syn.G2–3 Tg mice. **(D)** Representative immunoblots of pY143 parkin and parkin from anti-parkin immunoprecipitation samples of brainstem lysates and PARIS, PGC-1α, c-Abl, pY245 c-Abl, parkin, AIMP2, α-syn and β-actin in the detergent-soluble fractions of brainstem from 10-month-old symptomatic hA53T α-syn.G2–3 Tg mice compared to littermates. **(E)** Quantifications of PARIS, PGC-1α, AIMP2 and α-syn normalized to β-actin, and pY245 c-Abl normalized to c-Abl in D. **(F)** Quantifications of pY143 parkin normalized to immunoprecipitated parkin in D. **(G and I)** Representative immunoblots of α-syn, pS129 α-syn, pY39 α-syn and β-actin in the **(G)** detergent soluble and **(I)** detergent insoluble fractions of brainstem from 10-month-old symptomatic PARIS wild-type/hA53T α-syn.G2–3 Tg mice versus age-matched PARIS KO/hA53T α-syn.G2–3 Tg mice and littermate controls. The designated sample numbers in **D**, **F** and **H** indicate individual experimental animals. **(H and J)** Quantifications of α-syn monomer normalized to β-actin and pY39 α-syn and pS129 α-syn protein levels normalized to α-syn monomer in G and I. Data are from three independent experiments. Statistical significance was determined by one-way ANOVA with Sidak's post-test of multiple comparisons. The data are presented as the mean ± SEM. *$P < 0.05$, **$P < 0.01$, ***$P < 0.001$; ns = not significant; WT = wild-type.

selected for further characterization. To drive high expression specifically in the midbrain and to accelerate the potential pathology as previously described for TetP-AIMP2 mice (Lee *et al.*, 2013), the TetP-hA53T α-syn mice (line 4360) were stereotaxically injected into the ventral midbrain with AAV1-tTA-IRES-zsGreen (AAV-tTA) creating mice expressing high levels of hA53T α-syn in the midbrain (Supplementary Fig. 5G and H). These mice were treated with doxycycline or vehicle and immunoblot analysis reveals that AAV-tTA induces robust expression of hA53T α-syn in the ventral midbrain and that the transgene is sensitive to doxycycline (Supplementary Fig. 5G and H).

c-Abl contributes to α-syn-induced loss of parkin activity, and nigrostriatal degeneration in TetP-hA53T α-syn mice

To test the role of c-Abl in regulation of parkin activity and accumulation of parkin substrates in the ventral midbrain directly, the TetP-hA53T α-syn mice (line 4360) were crossbred to conditional c-Abl knockout mice to generate c-Abl KO/ TetP-hA53T α-syn mice (Fig. 4A) using a similar strategy that was used for the generation of c-Abl-KO/ hA53T α-syn.G2–3 Tg mice (Brahmachari *et al.*, 2016). The TetP-hA53T α-syn, TetP-hA53T α-syn/c-Abl KO and the non-transgenic mice were stereotaxically injected with AAV1-tTA-IRES-zsGreen to induce hA53T α-syn overexpression in the ventral midbrain (Fig. 4B). Equivalent levels of hA53T α-syn overexpression are observed in the AAV1-tTA-injected TetP-hA53T α-syn, TetP-hA53T α-syn/ c-Abl KO, while AAV1-tTA-injected non-transgenic mice do not express human A53T α-syn and serve as control (Fig. 4C and D). In addition, PARIS, PGC-1α, AIMP2, c-Abl, and pY245 c-Abl levels were monitored by immunoblot analysis, and parkin, pY143 parkin, and auto-ubiquitinated parkin levels were assessed by immunoprecipitation of parkin followed by immunoblot analysis (Fig. 4C–F). In the ventral midbrain of AAV1-tTA-injected TetP-hA53T α-syn mice there is a marked increase in c-Abl activity (pY245 c-Abl) accompanying significant elevation of tyrosine phosphorylation of parkin and profound reduction in auto-ubiquitinated parkin (Fig. 4C, E and F). Coincident with inactivation of parkin are significant elevations of PARIS and AIMP2, and reduction in PGC-1α (Fig. 4C and D). In contrast, in the AAV1-tTA-injected TetP-hA53T α-syn/c-Abl KO mice, the levels of pY143 parkin, auto-ubiquitinated parkin, PARIS, PGC-1α, and AIMP2 are restored to control levels (non-transgenic) (Fig. 4C–F). No change in PARIS and AIMP2 levels are observed in AAV1-tTA-injected non-transgenic mice (Fig. 4C and D). The ventral midbrain of the AAV1-tTA-injected TetP-hA53T α-syn, AAV1-tTA-injected TetP-hA53T α-syn /c-Abl KO and AAV1-tTA-injected non-transgenic mice were fractionated into detergent soluble and insoluble fractions (Fig. 4G–K)

Immunoblot of these fractions demonstrates that in the AAV1-tTA-injected TetP-hA53T α-syn mice there is accumulation of insoluble pS129 α-syn, pY39 α-syn and high molecular weight species of α-syn. No abnormalities are observed in the AAV1-tTA-injected non-transgenic mice. c-Abl KO significantly reduces the levels of insoluble pS129 α-syn, pY39 α-syn and high molecular weight species of α-syn (Fig. 4I and K). There is very mild accumulation of soluble pS129 α-syn and pY39 α-syn in the AAV1-tTA-injected TetP-hA53T α-syn and AAV1-tTA-injected TetP-hA53T α-syn /c-Abl KO mice, but no difference in their levels are observed among them (Fig. 4G and H).

Assessment of dopamine cell loss was evaluated by stereological analysis of TH and Nissl-positive neurons in the SNpc of TetP-hA53T α-syn, TetP-hA53T α-syn/c-Abl KO and non-transgenic mice injected with AAV1-tTA (Fig. 4L and M). Induction of hA53T α-syn in the SNpc led to robust loss of dopamine neurons (Fig. 4L and M), and an accompanying reduction in dopamine and its metabolites as determined by HPLC (Fig. 4N and Supplementary Fig. 6A–C); however, c-Abl KO significantly rescued the nigral degeneration of dopamine neurons and loss of dopamine (Fig. 4L–N). There was no loss of dopamine neurons and loss of dopamine in the AAV1-tTA-injected non-transgenic mice. Since the injection was unilateral, amphetamine-induced rotation was used as a functional behavioural readout of dopaminergic degeneration. Human A53T α-syn overexpression led to a significant increase in amphetamine-induced rotational behaviour consistent with the loss of dopamine neurons. c-Abl KO prevented the amphetamine-induced rotation indicating that the dopamine neurons were functionally spared (Fig. 4O). AAV1-tTA-injected non-transgenic mice did not rotate after amphetamine (Fig. 4O).

We examined the levels of other parkin E3 ligase substrates in TetP-hA53T α-syn mice, including STEP61, a cytoplasmic substrate upregulated in post-mortem Parkinson's disease brain (Kurup *et al.*, 2015), and the mitochondrial/mitophagy-related parkin substrates Miro1, mitofusin1 (Mfn1) and Bax (Glauser *et al.*, 2011; Charan *et al.*, 2014; Shlevkov *et al.*, 2016). The levels of STEP61, Miro1, Mfn1 and Bax were significantly elevated in the ventral midbrain of AAV1-tTA-injected TetP-hA53T mice (Supplementary Fig. 6D and E). c-Abl KO markedly reduced the level of the cytosolic substrate STEP61 similar to PARIS and AIMP2, but had no effect on the mitochondrial associated substrates, Miro1, Mfn1 and Bax (Supplementary Fig. 6D and E). The status of phospho S65-ubiquitin, an indicator mitochondrial recruitment of parkin and its activation, was also monitored. There was a partial reduction in the level of pS65-ubiquitin in the ventral midbrain of AAV1-tTA-injected TetP-hA53T mice that is partially restored by c-Abl KO (Supplementary Fig. 6F and G).
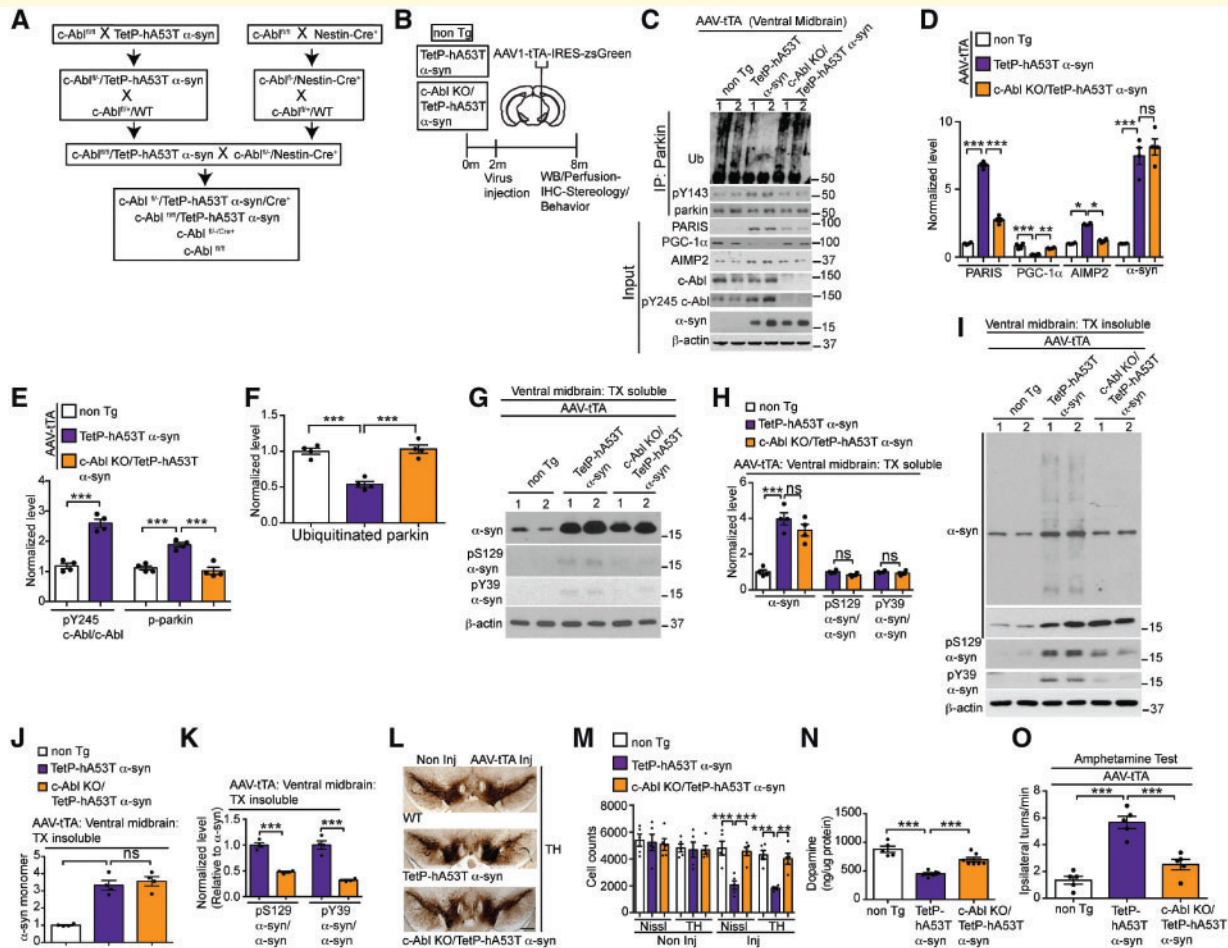
Figure 4 c-Abl knockout rescues parkin activity, reduces PARIS and AIMP2, prevents loss of dopamine neurons and α-syn pathology in TetP-hA53T α-syn mice. (A) Breeding strategy to generate c-Abl KO/TetP-hA53T α-syn mice. **(B)** Schematic of experiments for mice with stereotactic injection of AAV-tTA. **(C)** Representative immunoblots of ubiquitin, pY143 parkin, and parkin from anti-parkin immunoprecipitation samples of ventral midbrain lysates and PARIS, PGC-1α, c-Abl, pY245 c-Abl, AIMP2, α-syn, and β-actin in the ventral midbrain input samples from AAV-tTA-injected non-transgenic, TetP-hA53T α-syn and c-Abl KO/TetP-hA53T α-syn mice. **(D)** Quantifications of PARIS, PGC-1α, AIMP2, and α-syn protein levels normalized to β-actin from **C**. **(E)** pY245 c-Abl levels normalized to c-Abl, and pY143 parkin levels normalized to immunoprecipitated parkin in **C**. **(F)** Auto-ubiquitinated parkin normalized to immunoprecipitated parkin in **C**. **(C–F)** Data are from three independent experiments. **(G and I)** Representative immunoblots of α-syn, pY39 α-syn, pS129 α-syn and β-actin in the **(G)** detergent-soluble and **(I)** detergent-insoluble fractions of ventral midbrain lysates from AAV-tTA-injected c-Abl KO/TetP-hA53T α-syn and TetP-hA53T α-syn mice and age-matched littermate controls at 6-month post-injection. The designated sample numbers in **C**, **G** and **I** indicate individual experimental animals. **(H, J and K)** Quantification of **(H and J)** α-syn monomer normalized to β-actin, and **(H and K)** pY39 α-syn and pS129 α-syn protein levels normalized to α-syn monomer in **G** and **I**. **(L)** Representative TH immunostaining of midbrain sections from the SN of AAV-tTA-injected non-transgenic, TetP-hA53T α-syn and c-Abl KO/TetP-hA53T α-syn mice. Scale bars = 400 μm. **(M)** Stereological assessments of TH and Nissl-positive neurons in the SN of AAV-tTA-injected non-transgenic, TetP-hA53T α-syn and c-Abl KO/TetP-hA53T α-syn mice. **(N)** Striatal dopamine level as measured by HPLC. **(O)** Amphetamine-induced ipsilateral rotations in AAV-tTA-injected non-transgenic, TetP-hA53T α-syn and c-Abl KO/TetP-hA53T α-syn mice. Data are from three independent experiments. Statistical significance was determined by one-way ANOVA with Sidak's post-test of multiple comparisons. The data are presented as the mean ± SEM. *$P < 0.05$, **$P < 0.01$, ***$P < 0.001$; ns = not significant; WT = wild-type.

PARIS is a key mediator of α-syn-induced nigrostriatal degeneration in TetP-hA53T α-syn mice

To evaluate the role of PARIS in human A53T α-syn-induced nigrostriatal degeneration of dopamine neurons, the TetP-hA53T α-syn mice (line 4360) were crossed with

PARIS KO mice to create PARIS KO/TetP-hA53T α-syn mice (Fig. 5A). These TetP-hA53T α-syn and TetP-hA53T α-syn/PARIS KO mice were stereotaxically injected with AAV1-tTA-IRES-zsGreen to drive hA53T α-syn expression in the ventral midbrain (Fig. 5B). Equivalent levels of human A53T α-syn are observed in the AAV1-tTA-injected TetP-hA53T α-syn mice and the AAV1-tTA-injected TetP-
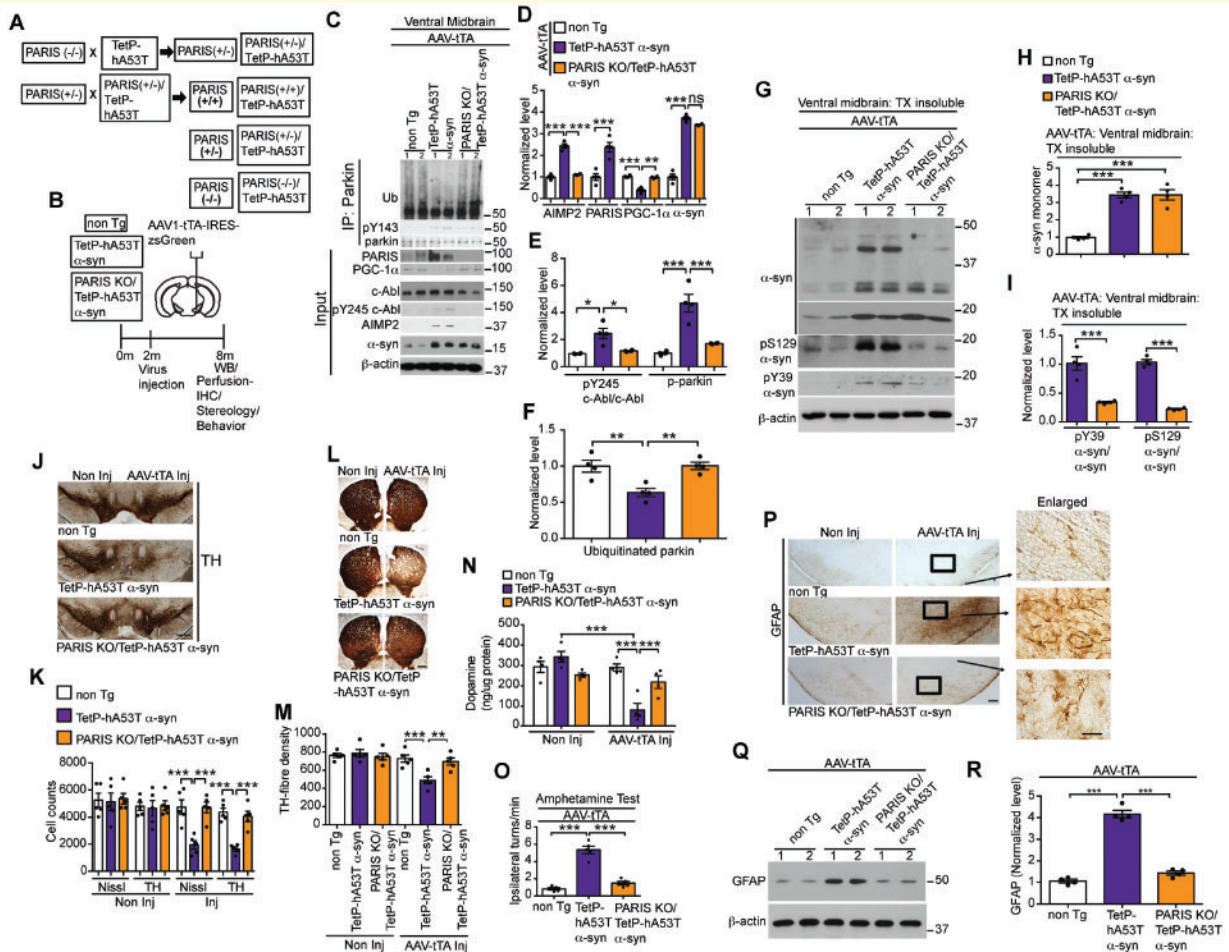
Figure 5 PARIS deletion rescues parkin activity and PGC-1α, reduces AIMP2, prevents loss of dopamine neurons and α-syn pathology in TetP-hA53T α-syn mice. (**A**) Breeding strategy to generate PARIS KO/TetP-hA53T α-syn mice. (**B**) Schematic of experiments for mice with stereotactic injection of AAV-tTA. (**C**) Representative immunoblots of ubiquitin, pY143 parkin, and parkin from anti-parkin immunoprecipitation samples of ventral midbrain lysates and representative immunoblots of PARIS, PGC-1α, c-Abl, pY245 c-Abl, AIMP2, α-syn, and β-actin in the ventral midbrain. Input samples from AAV-tTA-injected non-transgenic, TetP-hA53T α-syn and PARIS KO/TetP-hA53T α-syn mice. (**D**) Quantification of AIMP2, PARIS, PGC-1α and α-syn protein levels normalized to β-actin from **C**. (**E**) pY245 c-Abl levels normalized to c-Abl, and pY143 parkin levels normalized to immunoprecipitated parkin in **C**. (**F**) Auto-ubiquitinated parkin normalized to immunoprecipitated parkin in **C**. (**C**–**F**) Data are from three independent experiments. (**G**) Representative immunoblots of α-syn, pY39 α-syn, pS129 α-syn and β-actin in the detergent insoluble fractions of ventral midbrain lysates from AAV-tTA-injected PARIS KO/TetP-hA53T α-syn and TetP-hA53T α-syn mice, and age-matched littermate controls at 6-month post-injection. (**H** and **I**) Quantification of (**H**) α-syn monomer normalized to β-actin, and (**I**) pY39 α-syn and pS129 α-syn protein levels normalized to α-syn monomer in **G**. (**J**) Representative TH immunostaining of midbrain sections from the SN of AAV-tTA-injected non-transgenic, TetP-hA53T α-syn and PARIS KO/TetP-hA53T α-syn mice. Scale bars = 400 μm. (**K**) Stereological assessments of TH and Nissl-positive neurons in the SN of AAV-tTA-injected non-transgenic, TetP-hA53T α-syn and PARIS KO/TetP-hA53T α-syn mice. (**L**) Representative TH immunostaining of mouse striatal sections from AAV-tTA-injected non-transgenic, TetP-hA53T α-syn and PARIS KO/TetP-hA53T α-syn mice at 6-month post-injections. Scale bar = 200 μm. (**M**) Quantifications of dopaminergic fibre densities in the striatum by using ImageJ software. (**N**) Striatal dopamine level as measured by HPLC. (**O**) Amphetamine-induced ipsilateral rotations in AAV-tTA-injected non-transgenic, TetP-hA53T α-syn and PARIS KO/TetP-hA53T α-syn mice. (**P**) Representative GFAP immunohistochemistry of midbrain sections from the SN of AAV-tTA-injected non-transgenic, TetP-hA53T α-syn and PARIS KO/TetP-hA53T α-syn mice at 6-month post-injection (n = 3 mice per group). Enlarged images of the indicated regions are shown on the *right*. Scale bars = 400 μM; 50 μM (enlarged). (**Q**) Representative immunoblots of GFAP and β-actin in the ventral midbrain lysates from the AAV-tTA-injected non-transgenic, TetP-hA53T α-syn and PARIS KO/TetP-hA53T α-syn mice at 6 months post-injection. The designated sample numbers in **C**, **G**, and **Q** indicate individual experimental animals. (**R**) Quantifications for GFAP protein levels normalized to β-actin in **Q**. Data are from three independent experiments. Statistical significance was determined by one-way ANOVA with Sidak's post-test of multiple comparisons. The data are presented as the mean ± SEM. *$P < 0.05$, **$P < 0.01$, ***$P < 0.001$; ns = not significant; WT = wild-type.
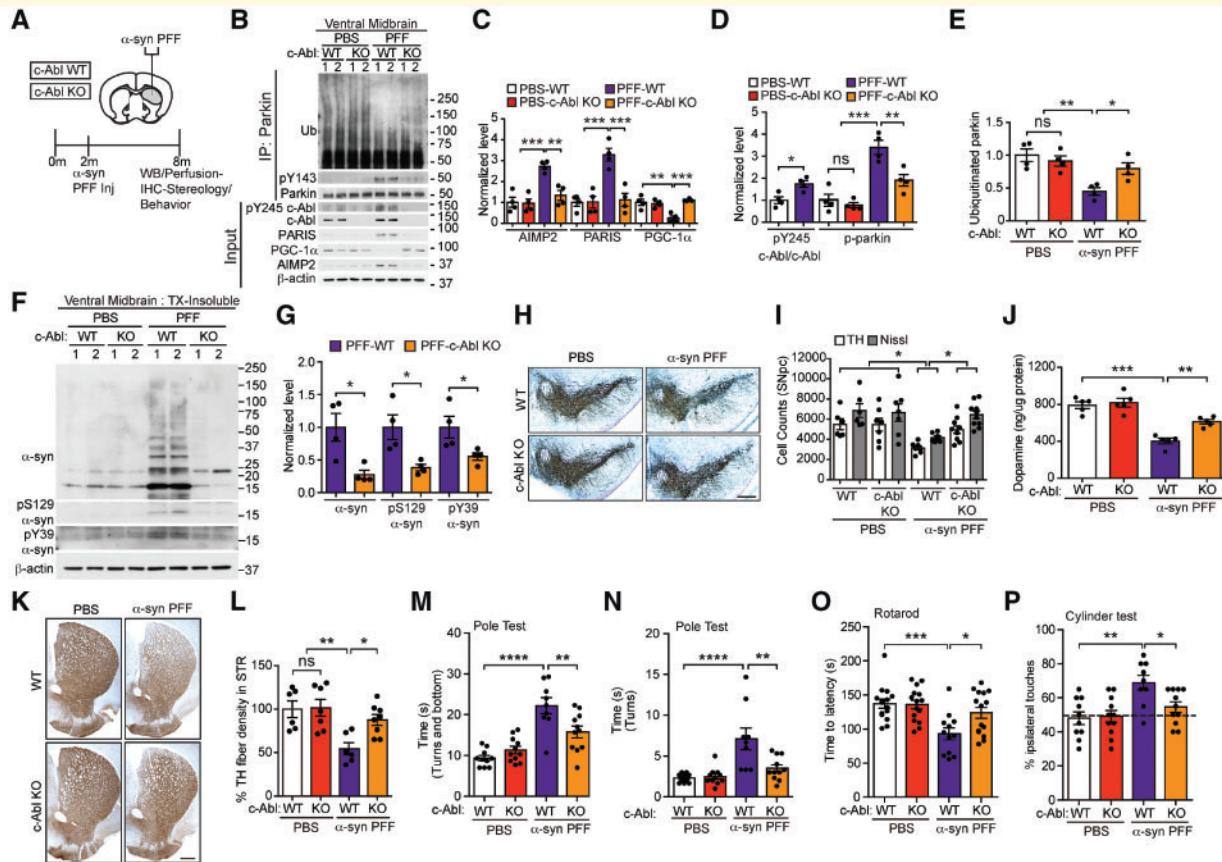
Figure 6 c-Abl knockout reduces α-syn-PFF-induced parkin inactivation and accumulations of PARIS and AIMP2 and neurodegeneration in wild-type mice. (**A**) Schematic of experiments for mice with stereotactic injection of α-syn-PFF. (**B**) Representative immunoblots of ubiquitin, pY143 parkin, and parkin from anti-parkin immunoprecipitation samples of ventral midbrain lysates and representative immunoblots of PARIS, c-Abl, pY245 c-Abl, AIMP2, PGC-1α, and β-actin in the ventral midbrain input samples from α-syn PFF- or PBS-injected wild-type and c-Abl KO mice. (**C**) Quantifications of AIMP2, PARIS, and PGC-1α protein levels normalized to β-actin from **B** (Tukey's post-test). (**D**) Quantifications of pY245 c-Abl normalized to c-Abl and pY143 parkin levels normalized to immunoprecipitated parkin in **B** (Tukey's post-test). (**E**) Quantifications of auto-ubiquitinated parkin normalized to immunoprecipitated parkin in **B** (Tukey's post-test). (**F**) Representative immunoblots of α-syn, pS129 α-syn, pY39 α-syn and β-actin in the detergent insoluble fractions of ventral midbrain lysates from wild-type and c-Abl KO mice injected with PBS or α-syn-PFF. The designated sample numbers in **B** and **F** indicate individual experimental animals. (**G**) Quantifications of α-syn monomer normalized to β-actin, and pS129 α-syn and pY39 α-syn protein levels normalized to β-actin in **F**. (unpaired two-tailed *t*-test). (**B–G**) Data are from three independent experiments. (**H**) Representative TH-immunostaining of midbrain sections from wild-type and c-Abl KO mice injected with α-syn PFFs or PBS. Scale bars = 400 μm. (**I**) Stereological assessments of TH- and Nissl-positive neurons in the SN of wild-type and c-Abl KO mice injected with PBS or α-syn PFF (Tukey's post-test). (**J**) Striatal dopamine levels as measured by HPLC (Sidak's post-test). (**K**) Representative TH immunostaining of mouse striatal sections from PBS or PFF-injected wild-type and c-Abl KO mice at 6-months post-injections. Scale bar = 200 μm. (**L**) Quantifications of dopaminergic fibre densities in the striatum by using ImageJ software (Tukey's post-test). (**M** and **N**) One hundred and eighty days after α-syn PFF injection, the Pole test measuring (**M**) time to turn and *bottom*, (**N**) total time to turn was performed in wild-type or c-Abl KO mice injected with PBS or α-syn PFF (Tukey's post-test). (**O** and **P**) One hundred and eighty days after α-syn PFF injection, (**O**) rotarod, and (**P**) cylinder tests were performed in wild-type or c-Abl KO mice injected with PBS or α-syn PFF (Tukey's post-test). Statistical significance was determined by Student's *t*-test or one-way ANOVA with indicated post-test of multiple comparisons as above. The data are presented as the mean ± SEM. *$P < 0.05$, **$P < 0.01$, ***$P < 0.001$, ****$P < 0.0001$; ns = not significant; WT = wild-type.

hA53T α-syn mice/PARIS KO mice (Fig. 5C and D). PARIS, PGC-1α, c-Abl, pY245 c-Abl, and AIMP2, were examined via immunoblot analysis (Fig. 5C–E). In addition, parkin, pY143 parkin, and auto-ubiquitinated parkin levels were examined by immunoprecipitation followed by immunoblot analysis (Fig. 5C, E and F). Knockout of PARIS in TetP-hA53T α-syn mice restored the levels of pY245 c-Abl, pY143 parkin, auto-ubiquitinated parkin, AIMP2, and

PGC-1α to control levels (non-transgenic) (Fig. 5C–F). No change in PARIS, PGC-1α, c-Abl, pY245 c-Abl, and AIMP2 levels were observed in AAV1-tTA-injected non-transgenic mice (Fig. 5C–F).

The ventral midbrain of the AAV1-tTA-injected TetP-hA53T α-syn, AAV1-tTA-injected TetP-hA53T α-syn/ PARIS KO and AAV1-tTA-injected non-transgenic mice were fractionated into detergent-soluble (Supplementary

Fig. 6H and I) and insoluble fractions (Fig. 5G–I). PARIS KO significantly reduces the levels of insoluble pS129 α-syn, pY39 α-syn and high molecular weight species of α-syn (Fig. 5G–I). There was mild accumulation of soluble pS129 α-syn and pY39 α-syn in the AAV1-tTA-injected TetP-hA53T α-syn and AAV1-tTA-injected TetP-hA53T α-syn/PARIS KO mice, but no difference in their levels are observed among them (Supplementary Fig. 6H and I).

Dopamine cell loss was monitored via stereological counting of TH and Nissl-stained neurons in the AAV1-tTA-injected TetP-hA53T α-syn and AAV1-tTA-injected AT/TetP-hA53T α-syn /PARIS KO mice and compared to AAV1-tTA-injected non-transgenic mice (Fig. 5J and K). As expected, induction of hA53T α-syn leads to robust loss of dopamine neurons (Fig. 5J and K), an accompanying reduction in striatal dopamine fibre density (Fig. 5L and M) and a reduction in dopamine and its metabolites as determined by HPLC (Fig. 5N and Supplementary Fig. 6J–L). However, PARIS KO significantly rescued the degeneration of dopamine neurons, loss of dopamine, and the loss of striatal dopamine fibre density (Fig. 5J–N). Similar to c-Abl KO, PARIS KO also prevents the amphetamine-induced rotation indicating that the dopamine neurons are functionally spared (Fig. 5O). There was a robust increase in the level of GFAP immunoreactivity in the AAV1-tTA-injected TetP-hA53T α-syn mice that is absent in the AAV1-tTA-injected TetP-hA53T α-syn/PARIS KO mice and AAV1-tTA-injected non-transgenic as determined by immunohistochemistry (Fig. 5P) and western blot analysis (Fig. 5Q and R). Similar to c-Abl KO, our analysis on STEP61, Miro1, Mfn1, and Bax reveals that PARIS KO reduces the upregulation of STEP61 in AAV-tTA-injected TetP-hA53T α-syn mice, but fails to have any effects on the levels of Mito1, Mfn1, and Bax (Supplementary Fig. 6M and N).

Taken together, our results indicate that parkin inactivation via tyrosine phosphorylation by c-Abl is a major event in degeneration of dopamine neurons in the ventral midbrain in response to the ventral midbrain induction of human A53T α-syn in the TetP-hA53T α-syn mice. This subsequently leads to accumulation of the parkin pathogenic substrates, PARIS and AIMP2, similar to our observations in hA53T α-syn.G2–3 Tg mice. PARIS in turn contributes to the human A53T α-syn-induced nigrostriatal degeneration of dopamine neurons.

c-Abl mediates α-syn PFF induced loss of DA neurons by reduction of parkin activity

Since the majority of Parkinson's disease is sporadic in nature, we then asked whether c-Abl-dependent parkin inactivation and accumulation PARIS also contributes to neurodegeneration relevant to sporadic Parkinson's disease. For these experiments the sporadic Parkinson's disease-relevant α-syn PFF mouse model that is driven, in part, via cell-to-cell transmission of pathological α-syn was used (Luk et al., 2012; Mao et al., 2016). To examine if c-Abl regulates parkin activity and accumulation of parkin substrates PARIS and AIMP2, wild-type and c-Abl KO mice were stereotaxically injected with α-syn PFFs or PBS into the dorsal striatum (Fig. 6A). c-Abl, pY245 c-Abl, PARIS, PGC-1α, and AIMP2, were examined via immunoblot analysis (Fig. 6B–D). In addition, parkin, pY143 parkin, and auto-ubiquitinated parkin levels were examined via immunoprecipitation followed by immunoblot analysis (Fig. 6B, D and E). In the ventral midbrain of α-syn PFF-injected wild-type mice, there is a marked increase in c-Abl activity (pY245 c-Abl), which is coincident with tyrosine phosphorylation of parkin, and a significant reduction in auto-ubiquitinated parkin (Fig. 6B, D and E). Accompanying the inactivation of parkin was a significant elevation of PARIS and AIMP2 and reduction in PGC-1α (Fig. 6B and C). In contrast, in the α-syn PFF-injected c-Abl KO mice, the levels of pY143 parkin, auto-ubiquitinated parkin, PARIS, AIMP2, and PGC-1α are almost at control levels (PBS-injected wild-type or c-Abl KO) (Fig. 6B–E). No change in pY143 parkin, auto-ubiquitinated parkin, PARIS, PGC-1α, and AIMP2 levels are observed in PBS-injected wild-type and c-Abl KO mice. The ventral midbrain of the PFF- and PBS-injected wild-type and c-Abl KO mice were fractionated into detergent-soluble (Supplementary Fig. 7A and B) and insoluble fractions (Fig. 6F and G). Immunoblot of these fractions demonstrates that in the α-syn PFF-injected wild-type mice there is accumulation of insoluble pS129 α-syn, pY39 α-syn and monomeric and high molecular weight species of α-syn. No abnormalities were observed in the PBS-injected wild-type and c-Abl KO mice. c-Abl KO dramatically reduced the levels of insoluble pS129 α-syn, pY39 α-syn and monomeric as well as high molecular weight species of α-syn (Fig. 6F and G). The soluble pS129 α-syn and pY39 α-syn were barely detectable in the PFF-injected wild-type and c-Abl KO mice and no difference in the levels of monomeric α-syn was observed among the cohorts (Supplementary Fig. 7A and B).

As reported previously (Luk et al., 2012; Mao et al., 2016), stereological counting of TH- and Nissl-positive neurons in the SNpc revealed significant loss of dopamine neurons in the wild-type mice at 180 days after injection of α-syn PFF (Fig. 6H and I). In contrast, there was a dramatic preservation of dopamine neurons in α-syn PFF-injected c-Abl KO mice (Fig. 6H and K). α-Syn PFF-injection also led to deficits in striatal dopamine and its metabolites as measured by HPLC (Fig. 6J and Supplementary Fig. 7C–E), and an accompanying reduction in striatal fibre density (Fig. 6K and L), while c-Abl KO significantly rescued the loss of dopamine and striatal fibre density (Fig. 6J–L). Consistent with earlier reports (Luk et al., 2012; Karuppagounder et al., 2014; Mao et al., 2016), wild-type mice injected with PFF show significant deficits in Pole test performance as evident from increased time to turn and time to reach the base (Fig. 6M and N). In contrast, α-syn PFF-injected c-Abl KO mice rescued these

deficits (Fig. 6M and N). Additionally, wild-type mice injected with α-syn PFFs display behavioural deficits as measured in rotarod and cylinder tests, while c-Abl KO mice injected with α-syn PFFs show no significant impairments in these tests (Fig. 6O and P).

Similar to the AAV1-tTA-injected TetP-hA53T α-syn mice, wild-type mice injected with α-syn PFFs led to a significant increase in the levels of STE61, Miro1, Mfn1 and Bax (Supplementary Fig. 7F and G). c-Abl deletion markedly restored the level of α-syn PFF-induced STE61 upregulation similar to PARIS and AIMP2, but failed to reduce the α-syn PFF-driven upregulation of Miro1, Mfn1 and Bax (Supplementary Fig. 7F and G). These results indicate that Miro1, Mfn1 and Bax likely do not directly contribute to nigrostriatal degeneration. Similar to the AAV1-tTA-injected TetP-hA53T α-syn mice, the levels of phospho-S65 ubiquitin were reduced in wild-type mice injected with α-syn PFFs compared to PBS-injected mice (Supplementary Fig. 7H and I). c-Abl KO mice injected with α-syn PFFs significantly prevented the reduction in the level of phospho-S65 ubiquitin (Supplementary Fig. 7H and I).

PARIS mediates α-syn preformed fibril-induced neurodegeneration

Finally, to examine if PARIS also regulates α-syn PFF-triggered neurodegeneration of dopamine neurons, wild-type and PARIS KO mice were stereotaxically injected with α-syn PFFs or PBS into the dorsal striatum (Fig. 7A). pY245 c-Abl, PARIS, PGC-1α and AIMP2 were examined by immunoblot analysis (Fig. 7B–D). In addition, parkin, pY143 parkin, and auto-ubiquitinated parkin levels were examined by immunoprecipitation followed by immunoblot analysis (Fig. 7B, D and E). Similar to c-Abl KO, knockout of PARIS markedly restored the levels of pY245 c-Abl, pY143 parkin, auto-ubiquitinated parkin, AIMP2, and PGC-1α to the control levels (PBS injected wild-type or PARIS KO) (Fig. 7B–E). No change in pY143 parkin, auto-ubiquitinated parkin, PARIS, PGC-1α, and AIMP2 levels were observed in PBS-injected wild-type and PARIS KO mice. The ventral midbrain of the PFF and PBS injected wild-type and PARIS KO mice were fractionated into detergent-soluble (Supplementary Fig. 7J and K) and insoluble fractions (Fig. 7F and G). Immunoblot of these fractions reveal that PARIS KO dramatically rescues the levels of insoluble pS129 α-syn, pY39 α-syn and monomeric as well as high molecular weight species of α-syn (Fig. 7F and G). No abnormalities are observed in the PBS injected wild-type and PARIS KO mice. The soluble pS129 α-syn and pY39 α-syn are barely detectable in the PFF injected wild-type and PARIS KO mice and no difference in the levels of monomeric α-syn is observed among the cohorts (Supplementary Fig. 7J and K).

Stereological counting of TH and Nissl-stained neurons in the SNpc of wild-type and PARIS KO mice injected with PBS or α-syn PFF reveals that PARIS KO dramatically rescues α-syn PFF-induced loss of dopamine neurons (Fig. 7H and I), striatal deficits of dopamine and its metabolites DOPAC and HVA, but not 3MT (Fig. 7J and Supplementary Fig. L–N), and reduction in dopamine fibre density (Fig. 7K and L) in wild-type mice. PARIS KO injected with α-syn PFFs are also resistant to behavioural abnormalities in the Pole test (Fig. 7M and N). Grip strength analysis indicates that wild-type mice injected with α-syn PFFs have reduced forelimb and all-limb strength (Mao *et al.*, 2016) (Fig. 7O and P); in contrast, PARIS KO prevents the loss of grip strength in mice (Fig. 7O and P). Similar to c-Abl KO, our analysis on mitochondrial/mitophagy-related parkin substrates and STEP61 reveals that PARIS KO reduces the upregulation of STEP61 in α-syn PFF-injected wild-type mice but fails to have any effects on the levels of Mito1, Mfn1 and Bax (Supplementary Fig. 7O and P). Consistent with c-Abl KO, deletion of PARIS significantly prevents the reduction of the levels of phospho-S65 ubiquitin in α-syn PFF injected mice (Supplementary Fig. 7Q and R).

Discussion

The major finding of this study is the observation that PARIS is a key contributor to α-syn-induced neurodegeneration. Knockout of PARIS reduces behavioural and neuropathological deficits, and prolongs the survival of the hA53T α-syn.G2–3 Tg mice by more than 5 months. PARIS KO also almost completely eliminates the neuropathological and behavioural abnormalities in the AAV1-tTA-injected TetP-hA53T α-syn mice and the α-syn PFF model. Thus, PARIS plays an important role in the degenerative process of both non-dopaminergic and dopaminergic neurons in Parkinson's disease. It also provides an underlying mechanism of how c-Abl activation contributes to the degenerative process through parkin inactivation and accumulation of the parkin substrate, PARIS, and confirms a role for c-Abl activation in α-syn-induced neurodegeneration (Ko *et al.*, 2010; Imam *et al.*, 2011; Hebron *et al.*, 2013; Gaki and Papavassiliou, 2014; Mahul-Mellier *et al.*, 2014; Brahmachari *et al.*, 2016; Lee *et al.*, 2017).

This study also provides further insights into the role of parkin inactivity or reduced activation in the pathogenesis of α-syn-induced neurodegeneration. Parkin inactivity or reduced activation leads to accumulation of the parkin substrates, AIMP2 and PARIS in the three different models of α-syn-induced neurodegeneration similar to what is observed in post-mortem substantia nigra in sporadic Parkinson's disease (Ko *et al.*, 2010; Imam *et al.*, 2011; Shin *et al.*, 2011). The role of AIMP2 could not be directly accessed since knockout of AIMP2 leads to embryonic lethality, but prior studies indicate that AIMP2 is a contributor to dopamine cell death in Parkinson's disease through activation of parthanatos (Lee *et al.*, 2013). On the other hand, knockout of PARIS in
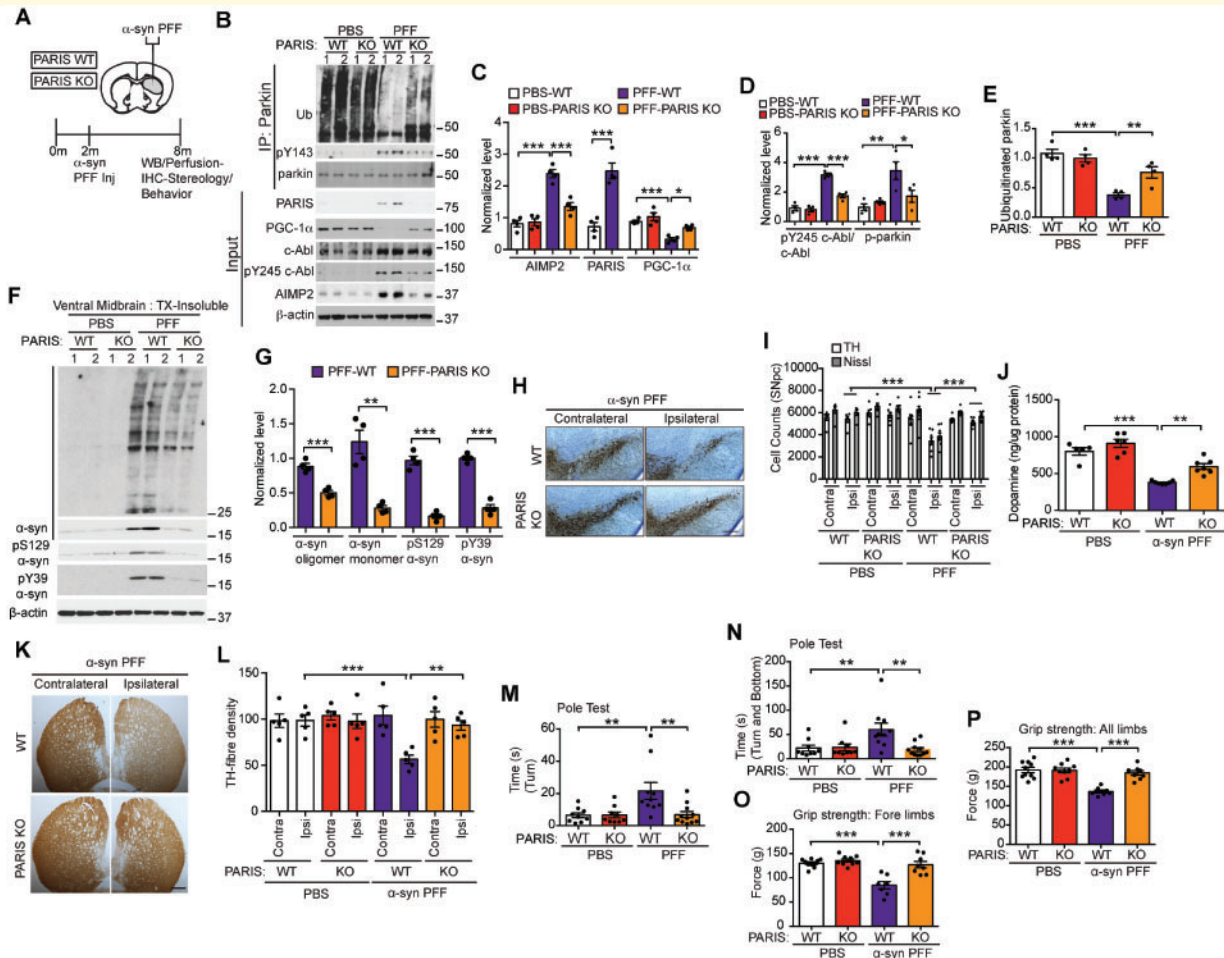
Figure 7 PARIS knockout reduces α-syn-PFF-induced parkin inactivation and neurodegeneration in wild-type mice.
(**A**) Schematic of experiments for mice with stereotactic injection of α-syn-PFF. (**B**) Representative immunoblots of ubiquitin, pY143 parkin, and parkin from anti-parkin immunoprecipitation samples of ventral midbrain lysates and representative immunoblots of PARIS, PGC-1α, c-Abl, pY245 c-Abl, AIMP2, and β-actin in the ventral midbrain Input samples from wild-type and PARIS KO mice injected with PBS or α-syn-PFF. (**C**) Quantification of AIMP2, PARIS, and PGC-1α protein levels normalized to β-actin from **B** (AIMP2: unpaired two-tailed *t*-test; PGC-1α: Sidak's post-test). (**D**) pY143 parkin levels normalized to immunoprecipitated parkin and pY245 c-Abl protein level normalized to c-Abl in **B** (Sidak's post-test). (**E**) Quantifications of auto-ubiquitinated parkin normalized to immunoprecipitated parkin in B (Sidak's post-test). (**F**) Representative immunoblots of α-syn oligomer, α-syn monomer, pS129 α-syn, pY39 α-syn and β-actin in the detergent insoluble fractions of ventral midbrain lysates from wild-type and PARIS KO mice injected with PBS or α-syn PFFs. The designated sample numbers in **B** and **F** indicate individual experimental animals. (**G**) Quantifications of α-syn, pS129 α-syn and pY39 α-syn protein levels normalized to β-actin in F (unpaired two-tailed *t*-test). (**B**–**G**) Data are from three independent experiments. (**H**) Representative TH immunostaining of midbrain sections from wild-type and PARIS KO mice injected with α-syn PFFs. Scale bars = 400 μm. (**I**) Stereological assessments of TH- and Nissl-positive neurons in the substantia nigra of wild-type and PARIS KO mice injected with PBS or α-syn PFFs (Sidak's post-test). (**K**) Representative TH immunostaining of mouse striatal sections from PFF-injected wild-type and PARIS KO mice at 6-months post-injections. Scale bar = 200 μm. (**L**) Quantifications of dopaminergic fibre densities in the striatum by using ImageJ software (Sidak's post-test). (**M** and **N**) Pole test measuring (**M**) time to turn, and total (**N**) time to turn and reach bottom was performed in wild-type or PARIS KO mice injected with PBS or α-syn PFFs (Sidak's post-test). (**O** and **P**) Grip strength test measuring force in (**O**) fore limbs and (**P**) all limbs in wild-type and PARIS KO mice injected with PBS or α-syn PFF (Sidak's post-test). Statistical significance was determined by one-way ANOVA with indicated post-test of multiple comparisons as above. Data are presented as the mean ± SEM. *$P < 0.05$, **$P < 0.01$, ***$P < 0.001$; ns = not significant; WT = wild-type.

wild-type mice does not have any discernible affects allowing the assessment of the absence of PARIS on α-syn-induced neurodegeneration. In three different models of α-syn-induced neurodegeneration knockout of PARIS is

profoundly protective, suggesting that PARIS elevation is key driver of α-syn-mediated loss of neurons.

Our results also provide an underlying mechanism of how c-Abl activation contributes to the degenerative

process in Parkinson's disease and α-syn-induced neurodegeneration through parkin inactivation and accumulation of the parkin substrate, PARIS, and confirms a role for c-Abl activation in α-synucleinopathy-induced neurodegeneration (Ko *et al.*, 2010; Imam *et al.*, 2011; Hebron *et al.*, 2013; Gaki and Papavassiliou, 2014; Mahul-Mellier *et al.*, 2014; Brahmachari *et al.*, 2016; Lee *et al.*, 2017). This study indicates that inactivation of parkin or maintaining parkin in an inactive state by c-Abl phosphorylation of parkin on tyrosine 143, plays a major role in α-syn-induced neurodegeneration. Consistent with the notion that c-Abl phosphorylation of parkin on tyrosine 143 is required for parkin inactivation are the observations that c-Abl fails to inhibit the E3 ligase activity of Y143F-parkin (Ko *et al.*, 2010; Imam *et al.*, 2011).

We also found that pathological α-syn expression leads to an inverse relationship between PARIS and PGC-1α levels, similar to what occurs in human post-mortem brain from patients with Parkinson's disease (Zheng *et al.*, 2010; Shin *et al.*, 2011; Stevens *et al.*, 2015). PARIS is a transcriptional repressor that kills dopamine neurons through down-regulation of PGC-1α in a mouse model of parkin inactivation (Siddiqui *et al.*, 2015, 2016), adult conditional knockouts of parkin (Shin *et al.*, 2011; Stevens *et al.*, 2015) or adult conditional knockdown of PINK1 (Lee *et al.*, 2017). Emerging evidence suggests that PGC-1α is critical for dopamine neuron survival (Zheng *et al.*, 2010; Mudo *et al.*, 2012; Ciron *et al.*, 2015; Jiang *et al.*, 2016). Thus, the downregulation of PGC-1α likely contributes to α-syn-induced neurodegeneration due to c-Abl activation, parkin inactivation and accumulation of PARIS. Thus, PARIS is a key mediator of neurodegeneration in familial and sporadic Parkinson's disease through regulation of PGC-1α. Our data also suggest a potential feed-forward mechanism that regulates the c-Abl-parkin-PARIS pathway in α-syn-induced neurodegeneration. It is evident from all three α-syn-induced neurodegeneration models that PARIS seems to act as both a downstream and upstream effector of the c-Abl-parkin pathway. We believe that once PARIS is upregulated by α-syn-induced c-Abl activation and parkin inactivation, it represses PGC-1α, leading to a decrease in mitochondrial biogenesis and subsequently increased oxidative stress (Stevens *et al.*, 2015). This oxidative stress, in turn, can activate c-Abl (Gonfloni *et al.*, 2012). Future experiments will be required to clarify these potential relationships.

We observed a downregulation of phospho-ubiquitin and an upregulation of the mitophagy-related parkin substrates Miro1, Mitofusin1 and Bax suggestive of defective mitophagy in the AAV1-tTA midbrain injected TetP-hA53T α-syn and the α-syn PFF injected mice. Miro1, Mitofusin1 and Bax likely don't play a role in degeneration of dopamine neurons in these models, as their levels fail to change in ventral midbrain after c-Abl or PARIS deletion, which rescues the loss of dopamine neurons. The partial restoration of phospho-ubiquitin by c-Abl or PARIS deletion indicates that ubiquitin phosphorylation at S65 may also

regulate cytosolic parkin activity consistent with the lowering the levels of cytosolic parkin substrates, PARIS, AIMP2 and STEP61. Consistent with this notion is the prior observation that cytosolic phospho-ubiquitin regulates the levels of PARIS (Lee *et al.*, 2017). Like PARIS and AIMP2, STEP61 is elevated in post-mortem Parkinson's disease brain (Kurup *et al.*, 2015). Future studies will be required to investigate the potential role of STEP61 in the degeneration of DA neurons.

In summary, the present study identifies PARIS as a key mediator of α-syn-induced neurodegeneration. PARIS plays a role in the neurodegeneration due to pathological α-syn in both non-dopaminergic and dopaminergic neurons. These results link c-Abl, parkin and PARIS in the pathogenesis of α-synucleinopathies in familial (A53T α-syn mutant) and sporadic Parkinson's disease. The near complete reversal of pathology and neurodegeneration by the knockout of PARIS indicates that strategies aimed at reducing or inhibiting PARIS could be a potent method to treat the neurodegeneration of Parkinson's disease and related α-synucleinopathies.

Acknowledgement

Funding

Competing interests

The value of patents owned by Valted, LLC could be affected by the study described in this article. Also, T.M.D. and V.L.D. are founders of Valted, LLC and hold an ownership equity interest in the company. This

arrangement has been reviewed and approved by the Johns Hopkins University in accordance with its conflict of interest policies.

Supplementary material

Supplementary material is available at *Brain* online.

References

Auluck PK, Caraveo G, Lindquist S. alpha-Synuclein: membrane interactions and toxicity in Parkinson's disease. Annu Rev Cell Dev Biol 2010; 26: 211–33.

Bezard E, Yue Z, Kirik D, Spillantini MG. Animal models of Parkinson's disease: limits and relevance to neuroprotection studies. Mov Disord 2013; 28: 61–70.

Bonifati V, Rizzu P, van Baren MJ, Schaap O, Breedveld GJ, Krieger E, et al. Mutations in the DJ-1 gene associated with autosomal recessive early-onset parkinsonism. Science 2003; 299: 256–9.

Bonnet AM, Jutras MF, Czernecki V, Corvol JC, Vidailhet M. Nonmotor symptoms in Parkinson's disease in 2012: relevant clinical aspects. Parkinsons Dis 2012; 2012: 198316.

Brahmachari S, Ge P, Lee SH, Kim D, Karuppagounder SS, Kumar M, et al. Activation of tyrosine kinase c-Abl contributes to alpha-synuclein-induced neurodegeneration. J Clin Invest 2016; 126: 2970–88.

Brasher BB, Van Etten RA. c-Abl has high intrinsic tyrosine kinase activity that is stimulated by mutation of the Src homology 3 domain and by autophosphorylation at two distinct regulatory tyrosines. J Biol Chem 2000; 275: 35631–7.

Charan RA, Johnson BN, Zaganelli S, Nardozzi JD, LaVoie MJ. Inhibition of apoptotic Bax translocation to the mitochondria is a central function of parkin. Cell Death Dis 2014; 5: e1313.

Chartier-Harlin MC, Kachergus J, Roumier C, Mouroux V, Douay X, Lincoln S, et al. Alpha-synuclein locus duplication as a cause of familial Parkinson's disease. Lancet 2004; 364: 1167–9.

Chesselet MF, Richter F. Modelling of Parkinson's disease in mice. Lancet Neurol 2011; 10: 1108–18.

Chung KK, Thomas B, Li X, Pletnikova O, Troncoso JC, Marsh L, et al. S-nitrosylation of parkin regulates ubiquitination and compromises parkin's protective function. Science 2004; 304: 1328–31.

Ciron C, Zheng L, Bobela W, Knott GW, Leone TC, Kelly DP, et al. PGC-1alpha activity in nigral dopamine neurons determines vulnerability to alpha-synuclein. Acta Neuropathol Commun 2015; 3: 16.

Corti O, Hampe C, Koutnikova H, Darios F, Jacquier S, Prigent A, et al. The p38 subunit of the aminoacyl-tRNA synthetase complex is a Parkin substrate: linking protein biosynthesis and neurodegeneration. Hum Mol Genet 2003; 12: 1427–37.

Corti O, Lesage S, Brice A. What genetics tells us about the causes and mechanisms of Parkinson's disease. Physiol Rev 2011; 91: 1161–218.

Dauer W, Przedborski S. Parkinson's disease: mechanisms and models. Neuron 2003; 39: 889–909.

Dawson TM, Dawson VL. Parkin plays a role in sporadic Parkinson's disease. Neurodegener Dis 2014; 13: 69–71.

Dawson TM, Ko HS, Dawson VL. Genetic animal models of Parkinson's disease. Neuron 2010; 66: 646–61.

Deng H, Yuan L. Genetic variants and animal models in SNCA and Parkinson disease. Ageing Res Rev 2014; 15: 161–76.

Di Fonzo A, Rohe CF, Ferreira J, Chien HF, Vacca L, Stocchi F, et al. A frequent LRRK2 gene mutation associated with autosomal dominant Parkinson's disease. Lancet 2005; 365: 412–5.

Di Fonzo A, Wu-Chou YH, Lu CS, van Doeselaar M, Simons EJ, Rohe CF, et al. A common missense variant in the LRRK2 gene, Gly2385Arg, associated with Parkinson's disease risk in Taiwan. Neurogenetics 2006; 7: 133–8.

Eiyama A, Okamoto K. PINK1/Parkin-mediated mitophagy in mammalian cells. Curr Opin Cell Biol 2015; 33: 95–101.

Fedorowicz MA, de Vries-Schneider RL, Rub C, Becker D, Huang Y, Zhou C, et al. Cytosolic cleaved PINK1 represses Parkin translocation to mitochondria and mitophagy. EMBO Rep 2014; 15: 86–93.

Fernagut PO, Chesselet MF. Alpha-synuclein and transgenic mouse models. Neurobiol Dis 2004; 17: 123–30.

Fiesel FC, Ando M, Hudec R, Hill AR, Castanedes-Casey M, Caulfield TR, et al. (Patho-)physiological relevance of PINK1-dependent ubiquitin phosphorylation. EMBO Rep 2015; 16: 1114–30.

Gaki GS, Papavassiliou AG. Oxidative stress-induced signaling pathways implicated in the pathogenesis of Parkinson's disease. Neuromolecular Med 2014; 16: 217–30.

Glauser L, Sonnay S, Stafa K, Moore DJ. Parkin promotes the ubiquitination and degradation of the mitochondrial fusion factor mitofusin 1. J Neurochem 2011; 118: 636–45.

Goedert M. Alpha-synuclein and neurodegenerative diseases. Nat Rev Neurosci 2001; 2: 492–501.

Goedert M, Spillantini MG, Del Tredici K, Braak H. 100 years of Lewy pathology. Nat Rev Neurol 2013; 9: 13–24.

Gonfloni S, Maiani E, Di Bartolomeo C, Diederich M, Cesareni G. Oxidative Stress, DNA damage, and c-Abl Signaling: at the crossroad in neurodegenerative diseases? Int J Cell Biol 2012; 2012: 683097.

Hebron ML, Lonskaya I, Moussa CE. Nilotinib reverses loss of dopamine neurons and improves motor behavior via autophagic degradation of alpha-synuclein in Parkinson's disease models. Hum Mol Genet 2013; 22: 3315–28.

Hernandez DG, Reed X, Singleton AB. Genetics in Parkinson disease: Mendelian versus non-Mendelian inheritance. J Neurochem 2016; 139 (Suppl 1): 59–74.

Imai Y, Soda M, Takahashi R. Parkin suppresses unfolded protein stress-induced cell death through its E3 ubiquitin-protein ligase activity. J Biol Chem 2000; 275: 35661–4.

Imam SZ, Zhou Q, Yamamoto A, Valente AJ, Ali SF, Bains M, et al. Novel regulation of parkin function through c-Abl-mediated tyrosine phosphorylation: implications for Parkinson's disease. J Neurosci 2011; 31: 157–63.

Jiang H, Kang SU, Zhang S, Karuppagounder S, Xu J, Lee YK, et al. Adult conditional knockout of PGC-1alpha leads to loss of dopamine neurons. eNeuro 2016; 3. doi: 10.1523/ENEURO.0183-16.2016.

Karuppagounder SS, Brahmachari S, Lee Y, Dawson VL, Dawson TM, Ko HS. The c-Abl inhibitor, nilotinib, protects dopaminergic neurons in a preclinical animal model of Parkinson's disease. Sci Rep 2014; 4: 4874.

Kim MJ, Park BJ, Kang YS, Kim HJ, Park JH, Kang JW, et al. Downregulation of FUSE-binding protein and c-myc by tRNA synthetase cofactor p38 is required for lung cell differentiation. Nat Genet 2003; 34: 330–6.

Kitada T, Asakawa S, Hattori N, Matsumine H, Yamamura Y, Minoshima S, et al. Mutations in the parkin gene cause autosomal recessive juvenile parkinsonism. Nature 1998; 392: 605–8.

Kitada T, Pisani A, Porter DR, Yamaguchi H, Tscherter A, Martella G, et al. Impaired dopamine release and synaptic plasticity in the striatum of PINK1-deficient mice. Proc Natl Acad Sci USA 2007; 104: 11441–6.

Ko HS, Lee Y, Shin JH, Karuppagounder SS, Gadad BS, Koleske AJ, et al. Phosphorylation by the c-Abl protein tyrosine kinase inhibits parkin's ubiquitination and protective function. Proc Natl Acad Sci USA 2010; 107: 16691–6.

Ko HS, von Coelln R, Sriram SR, Kim SW, Chung KK, Pletnikova O, et al. Accumulation of the authentic parkin substrate aminoacyl-tRNA synthetase cofactor, p38/JTV-1, leads to catecholaminergic cell death. J Neurosci 2005; 25: 7968–78.

Kruger R, Kuhn W, Muller T, Woitalla D, Graeber M, Kosel S, et al. Ala30Pro mutation in the gene encoding alpha-synuclein in Parkinson's disease. Nat Genet 1998; 18: 106–8.

Kuo YM, Li Z, Jiao Y, Gaborit N, Pani AK, Orrison BM, et al. Extensive enteric nervous system abnormalities in mice transgenic for artificial chromosomes containing Parkinson disease-associated alpha-synuclein gene mutations precede central nervous system changes. Hum Mol Genet 2010; 19: 1633–50.

Kurup PK, Xu J, Videira RA, Ononenyi C, Baltazar G, Lombroso PJ, et al. STEP61 is a substrate of the E3 ligase parkin and is upregulated in Parkinson's disease. Proc Natl Acad Sci USA 2015; 112: 1202–7.

Lashuel HA, Overk CR, Oueslati A, Masliah E. The many faces of alpha-synuclein: from structure and toxicity to therapeutic target. Nat Rev Neurosci 2013; 14: 38–48.

LaVoie MJ, Ostaszewski BL, Weihofen A, Schlossmacher MG, Selkoe DJ. Dopamine covalently modifies and functionally inactivates parkin. Nat Med 2005; 11: 1214–21.

Lee MK, Stirling W, Xu Y, Xu X, Qui D, Mandir AS, et al. Human alpha-synuclein-harboring familial Parkinson's disease-linked Ala-53 –> Thr mutation causes neurodegenerative disease with alpha-synuclein aggregation in transgenic mice. Proc Natl Acad Sci USA 2002; 99: 8968–73.

Lee VM, Trojanowski JQ. Mechanisms of Parkinson's disease linked to pathological alpha-synuclein: new targets for drug discovery. Neuron 2006; 52: 33–8.

Lee Y, Dawson VL, Dawson TM. Animal models of Parkinson's disease: vertebrate genetics. Cold Spring Harb Perspect Med 2012; 2. doi: 10.1101/cshperspect.a009324.

Lee Y, Karuppagounder SS, Shin JH, Lee YI, Ko HS, Swing D, et al. Parthanatos mediates AIMP2-activated age-dependent dopaminergic neuronal loss. Nat Neurosci 2013; 16: 1392–400.

Lee Y, Stevens DA, Kang SU, Jiang H, Lee YI, Ko HS, et al. PINK1 primes Parkin-mediated ubiquitination of PARIS in dopaminergic neuronal survival. Cell Rep 2017; 18: 918–32.

Luk KC, Kehm V, Carroll J, Zhang B, O'Brien P, Trojanowski JQ, et al. Pathological alpha-synuclein transmission initiates Parkinson-like neurodegeneration in nontransgenic mice. Science 2012; 338: 949–53.

Mahul-Mellier AL, Fauvet B, Gysbers A, Dikiy I, Oueslati A, Georgeon S, et al. c-Abl phosphorylates alpha-synuclein and regulates its degradation: implication for alpha-synuclein clearance and contribution to the pathogenesis of Parkinson's disease. Hum Mol Genet 2014; 23: 2858–79.

Mao X, Ou MT, Karuppagounder SS, Kam TI, Yin X, Xiong Y, et al. Pathological alpha-synuclein transmission initiated by binding lymphocyte-activation gene 3. Science 2016; 353. doi: 10.1126/science.aah3374.

Maries E, Dass B, Collier TJ, Kordower JH, Steece-Collier K. The role of alpha-synuclein in Parkinson's disease: insights from animal models. Nat Rev Neurosci 2003; 4: 727–38.

Martin I, Dawson VL, Dawson TM. Recent advances in the genetics of Parkinson's disease. Annual review of genomics and human genetics 2011; 12: 301–25.

Mudo G, Makela J, Di Liberto V, Tselykh TV, Olivieri M, Piepponen P, et al. Transgenic expression and activation of PGC-1alpha protect dopaminergic neurons in the MPTP mouse model of Parkinson's disease. Cell Mol Life Sci 2012; 69: 1153–65.

O'Gorman S, Dagenais NA, Qian M, Marchuk Y. Protamine-Cre recombinase transgenes efficiently recombine target sequences in the male germ line of mice, but not in embryonic stem cells. Proc Natl Acad Sci USA 1997; 94: 14602–7.

Panicker N, Dawson VL, Dawson TM. Activation mechanisms of the E3 ubiquitin ligase parkin. Biochem J 2017; 474: 3075–86.

Polymeropoulos MH, Lavedan C, Leroy E, Ide SE, Dehejia A, Dutra A, et al. Mutation in the alpha-synuclein gene identified in families with Parkinson's disease. Science 1997; 276: 2045–7.

Ramirez A, Heimbach A, Grundemann J, Stiller B, Hampshire D, Cid LP, et al. Hereditary parkinsonism with dementia is caused by mutations in ATP13A2, encoding a lysosomal type 5 P-type ATPase. Nat Genet 2006; 38: 1184–91.

Ross OA, Wu YR, Lee MC, Funayama M, Chen ML, Soto AI, et al. Analysis of Lrrk2 R1628P as a risk factor for Parkinson's disease. Ann Neurol 2008; 64: 88–92.

Satake W, Nakabayashi Y, Mizuta I, Hirota Y, Ito C, Kubo M, et al. Genome-wide association study identifies common variants at four loci as genetic risk factors for Parkinson's disease. Nat Genet 2009; 41: 1303–7.

Savitt JM, Dawson VL, Dawson TM. Diagnosis and treatment of Parkinson disease: molecules to medicine. J Clin Invest 2006; 116: 1744–54.

Scarffe LA, Stevens DA, Dawson VL, Dawson TM. Parkin and PINK1: much more than mitophagy. Trends Neurosci 2014; 37: 315–24.

Shin JH, Ko HS, Kang H, Lee Y, Lee YI, Pletinkova O, et al. PARIS (ZNF746) repression of PGC-1alpha contributes to neurodegeneration in Parkinson's disease. Cell 2011; 144: 689–702.

Shlevkov E, Kramer T, Schapansky J, LaVoie MJ, Schwarz TL. Miro phosphorylation sites regulate Parkin recruitment and mitochondrial motility. Proc Natl Acad Sci USA 2016; 113: E6097–E106.

Shulman JM, De Jager PL, Feany MB. Parkinson's disease: genetics and pathogenesis. Annu Rev Pathol 2011; 6: 193–222.

Siddiqui A, Bhaumik D, Chinta SJ, Rane A, Rajagopalan S, Lieu CA, et al. Mitochondrial Quality control via the PGC1alpha-TFEB signaling pathway is compromised by Parkin Q311X mutation but independently restored by Rapamycin. J Neurosci 2015; 35: 12833–44.

Siddiqui A, Rane A, Rajagopalan S, Chinta SJ, Andersen JK. Detrimental effects of oxidative losses in parkin activity in a model of sporadic Parkinson's disease are attenuated by restoration of PGC1alpha. Neurobiol Dis 2016; 93: 115–20.

Sidransky E, Nalls MA, Aasly JO, Aharon-Peretz J, Annesi G, Barbosa ER, et al. Multicenter analysis of glucocerebrosidase mutations in Parkinson's disease. N Engl J Med 2009; 361: 1651–61.

Simon-Sanchez J, Schulte C, Bras JM, Sharma M, Gibbs JR, Berg D, et al. Genome-wide association study reveals genetic risk underlying Parkinson's disease. Nat Genet 2009; 41: 1308–12.

Singleton AB, Farrer M, Johnson J, Singleton A, Hague S, Kachergus J, et al. alpha-Synuclein locus triplication causes Parkinson's disease. Science 2003; 302: 841.

Stevens DA, Lee Y, Kang HC, Lee BD, Lee YI, Bower A, et al. Parkin loss leads to PARIS-dependent declines in mitochondrial mass and respiration. Proc Natl Acad Sci USA 2015; 112: 11696–701.

Unger EL, Eve DJ, Perez XA, Reichenbach DK, Xu Y, Lee MK, et al. Locomotor hyperactivity and alterations in dopamine neurotransmission are associated with overexpression of A53T mutant human alpha-synuclein in mice. Neurobiol Dis 2006; 21: 431–43.

Valente EM, Abou-Sleiman PM, Caputo V, Muqit MM, Harvey K, Gispert S, et al. Hereditary early-onset Parkinson's disease caused by mutations in PINK1. Science 2004; 304: 1158–60.

Vilarino-Guell C, Wider C, Ross OA, Dachsel JC, Kachergus JM, Lincoln SJ, et al. VPS35 mutations in Parkinson disease. Am J Hum Genet 2011; 89: 162–7.

West MJ. New stereological methods for counting neurons. Neurobiol Aging 1993; 14: 275–85.

Yao D, Gu Z, Nakamura T, Shi ZQ, Ma Y, Gaston B, et al. Nitrosative stress linked to sporadic Parkinson's disease: S-nitrosylation of parkin regulates its E3 ubiquitin ligase activity. Proc Natl Acad Sci USA 2004; 101: 10810–4.

Yun SP, Kam TI, Panicker N, Kim S, Oh Y, Park JS, et al. Block of A1 astrocyte conversion by microglia is neuroprotective in models of Parkinson's disease. Nat Med 2018; 24: 931–8.

Zarranz JJ, Alegre J, Gomez-Esteban JC, Lezcano E, Ros R, Ampuero I, et al. The new mutation, E46K, of alpha-synuclein causes Parkinson and Lewy body dementia. Ann Neurol 2004; 55: 164–73.

Zhang Y, Gao J, Chung KK, Huang H, Dawson VL, Dawson TM. Parkin functions as an E2-dependent ubiquitin- protein ligase and promotes the degradation of the synaptic vesicle-associated protein, CDCrel-1. Proc Natl Acad Sci USA 2000; 97: 13354–9.

Zheng B, Liao Z, Locascio JJ, Lesniak KA, Roderick SS, Watt ML, et al. PGC-1alpha, a potential therapeutic target for early intervention in Parkinson's disease. Sci Transl Med 2010; 2: 52ra73.

Zimprich A, Benet-Pages A, Struhal W, Graf E, Eck SH, Offman MN, et al. A mutation in VPS35, encoding a subunit of the retromer complex, causes late-onset Parkinson disease. Am J Hum Genet 2011; 89: 168–75.

Zimprich A, Biskup S, Leitner P, Lichtner P, Farrer M, Lincoln S, et al. Mutations in LRRK2 cause autosomal-dominant parkinsonism with pleomorphic pathology. Neuron 2004; 44: 601–7.